FLUID MODELING OF EXHAUST GAS DISPERSION FOR THE UNIVERSITY OF COLORADO HEALTH SCIENCES CENTER

Final Report
(June 1989 - August 1989)

Prepared by

Thomas Z. Tan*
Robert N. Meroney+

for

Physical Plant and Maintenance Department
University of Colorado Health Sciences Center
Denver, Colorado 80262

* Research Associate
+ Professor, Civil Engineering

FLUID MECHANICS AND WIND ENGINEERING PROGRAM

Colorado State University

CSU Contract No. 2-97850
CER88-89TZT-RNM-17

ABSTRACT

A wind-tunnel measurement program was performed to evaluate the influence of building and plume aerodynamics on plume dilution for the University of Colorado Health Sciences Center (UCHSC). Data is reported in terms of normalized concentrations (K coefficients) to permit concentration estimates for alternative traffic, exhaust and wind speed conditions. Concentrations can be estimated for alternative configurations, but acceptability must depend upon current air-quality standards.

ACKNOWLEDGEMENTS

The authors wish to express their gratitude to the staff and personnel of the Fluid Dynamics and Diffusion Laboratory at Colorado State University. Special thanks go to Mr. Q. Roberts and Mr. D. Parce who built the 1:150 scale model, and Mr. D. Parce who assisted during flow visualization and concentration data acquisition.

TABLE OF CONTENTS

LIST OF TABLES

LIST OF FIGURES

LIST OF SYMBOLS

A,B,C	Constants
BR	Blockage ratio
C_p	Specific heat capacity at constant pressure
E	Hot wire voltage output
h	Height of the obstacle
g	Gravitational acceleration
k	Roughness length
L	Length
Q	Flow rate
S	Distance downstream of the obstacle
T	Temperature
U	Wind velocity
u_*	Friction velocity
X	Concentration
x	Distance
Z	Height above ground
z_o	Roughness length

Greek Characters

ρ	Air density
Γ	Abiabatic potential temperature lapse rate
κ	Thermal conductivity
μ	Dynamic viscosity
ν	Kinematic viscosity
ρ	Density
χ	Fraction of a gas component
Ω	Angular velocity of earth - $0.726*10^{-4}$ rad/s

Dimensionless Parameters

Ec	Eckert number
Ma	Mach number
Re	Reynolds number
Ri	Bulk Richardson number
Ro	Rossby number
Pr	Prandtl number
V	Volume flux ratio ($Q/U_H L^2$)

1 INTRODUCTION

The Physical Plant and Maintenance Department, University of Colorado Health Sciences Center (UCHSC), must plan for adequate ventilation of the School of Medicine. Ventilation and air handling units housing the fans and ancillary equipment, air intakes and exhaust vents have to be carefully placed to avoid future odor problems.

A problem exists concerning the current operation of the UCHSC ventilation system. Exhaust fumes from seed storage and drying operations, animal pens, and chemical fume hoods are released at many points over the roofs of the UCHSC. Occasionally these fumes enter the air-handling units resulting in odors and contaminated air throughout the School of Medicine. Another problem is to decide where are the best locations for the inlet ventilators for the new Biomedical Research Center (BRC) in order to avoid vehicle exhaust entrainment.

Measurements were separately carried out for a Phase 1 series of tests oriented on the School of Medicine and a Phase 2 series of tests oriented on the Biomedical Research Center. Each phase consisted of two groups of tests as outlined below:

Group 1A: Smoke visualization of the trajectories and dispersion from three exhaust locations distributed over the roofs of the UCHSC and near the Research Bridge, and

Group 1B: Concentration measurements over the roof and at air-handler inlets and other locations concerned.

Group 2A: Smoke visualization of the trajectories and dispersion from two exhaust locations distributed over the roofs of the BRC, and the exhaust caused by the traffic at Colorado Boulevard, and the exhaust located on the roof of the Research Bridge,

Group 2B: Concentration measurements over the locations of potential ventilator inlets located around the UCHSC BRC.

This report summarizes the results from a wind tunnel simulation of gaseous plume dispersion over the UCHSC complex (see Figure 1). Visualization and concentration measurements are renewed to identify flow behavior and identify troublesome inlet locations.

2 MODELING OF PLUME DISPERSION FROM VENTILATOR SITES

The Appendix describes in general terms the scaling laws that cover a large class of fluid modeling applications. The intent of this section is to specifically address the modeling techniques used in the present study.

The exhaust air released from the tunnel ventilators will exit at ambient temperatures and densities; hence, the source gas used in the model was primarily nitrogen released at room temperatures (specific gravity ≈ 1.0). Thus the plume mass flux, momentum flux and volume flux are essentially equivalent ratios, and the plume Froude number is not a relevant parameter.

The wind approaches the Denver city over suburban roughness. Replicas (at reduced scale of 1:150) of all buildings within 900 feet of the School of Medicine were constructed and placed on the downwind turntable in the wind tunnel. The wind characteristics approaching the UCHSC center site were simulated with a generic suburban roughness constructed from one-inch cubes.

The modeling parameter decision process yielded the following conclusions:

1. Maximum field dispersion distance of interest and size of the FDDL Environmental Wind Tunnel facility resulted in the selection of a 1:150 model length scale ratio.

2. Neutral stratification in the laboratory was used to reproduce the dispersion dynamics.

3. Wind-tunnel floor roughness was adjusted to produce properly scaled wind shear and turbulent structure.

4. Model wind speed and stack exit velocity were set at large enough magnitudes to assure Reynolds number independence of approach flow and stack flow.

5. Model wind velocity to plume velocity ratios were set equal to the field values; thus assuring similarity of plume trajectories.

3 DATA ACQUISITION AND ANALYSIS TECHNIQUES

Laboratory measurement techniques are discussed in this section, along with conversion methods used to relate measured model quantities to their meaningful field equivalents. Some of the methods used are conventional and need little elaboration.

3.1 Wind Tunnel Facilities

The experiments were performed in the Environmental Wind Tunnel (EWT) shown in Figure 2. This wind tunnel, especially designed to study atmospheric flow phenomena, incorporates special features such as an adjustable ceiling, a rotating turntable and a long test section to permit adequate reproduction of micrometeorological behavior. Mean wind speeds of 0.1 to 15 m/sec in the EWT can be obtained. Boundary-layer thickness up to 1.2 m can be developed "naturally" over the downstream 6 m of the EWT test section by using vortex generators at the test section entrance and surface roughness on the floor. The flexible test section on the EWT roof is adjustable in height to permit the longitudinal pressure gradient to be set at zero.

3.2 Wind Profile Measurements

Velocity measurements were made with single-hot-film probes and anemometry equipment manufactured by Thermo-System, Inc. (TSI).

Velocity Standard

The velocity standard used in the present study consisted of a Matheson Model 8116-0154 mass flowmeter and a profile conditioning section designed and calibrated by the Fluid Dynamics and Diffusion (FDDL) staff at Colorado State University (CSU). The mass flowmeter measures mass flow rate independent of temperature and pressure. The profile conditioning section forms a flat velocity profile of very low turbulence at the position where the hot-film-probe is located. Incorporating a measurement of the ambient atmospheric pressure, temperature and a profile correction factor permits the calibration of velocity at the measurement station from 0.15-2.2 m/s to within ± 5 percent.

Single-Hot-Film Probe Measurements

Single-hot-film (TSI 1210 Sensor) measurements were used to document the longitudinal turbulence levels for the approach flow conditions. During calibration the probe voltages were recorded at several velocities covering the range of interest. These voltage-velocity (E,U) pairs were then regressed to the equation $E^2 = A + BU^c$ via a least squares approach for various assumed values of the exponent c. Convergence to the minimum residual error was accelerated by using the secant method to find the best new estimate for the exponent c.

The hot-film-probe was mounted on a vertical traverse and positioned over the measurement location in the wind tunnel. The anemometer's output

voltage was digitized and stored within an IBM AT computer. This voltage time series was converted to a velocity time series using the inverse of the calibration equation; $U = [(E^2 - A)/B]^{1/c}$. The velocity time series was then analyzed for pertinent statistical quantities, such as mean velocity and root-mean-square turbulent velocity fluctuations. The computer system would move the velocity probe to a vertical position, acquire the data, then move on to the next vertical positions; thus obtaining an entire vertical velocity profile automatically.

Error Statement

The calibration curve yielded hot film anemometer velocities that were always within 2 percent of the known calibrator velocity. Considering the accumulative effect of calibrator, calibration curve fit and other errors the model velocity time series should be accurate to within 10 percent.

3.3 Flow Visualization Techniques

A visible plume was produced by passing the metered simulant gas through a smoke generator (Fog/Smoke Machine manufactured by Roscolab, Ltd.) and then out of the modeled stack. The visible plumes for each test were recorded on either VHS or S-VHS video cassettes with a Panasonic Professional/Industrial camera/recorder system (AG-450). Run number titles were placed on the video cassette with a title generator.

3.4 Concentration Measurements

The experimental measurements of concentration were performed using a Hewlett Packard gas-chromatograph and sampling systems designed by Fluid Dynamics and Diffusion Laboratory staff.

3.4.1 *Gas Chromatograph*

A gas chromatograph (Hewlett-Packard Model 5710A) (GC) with flame ionization detector (FID) operates on the principle that the electrical conductivity of a gas is directly proportional to the concentration of charged particles within the gas. The ions in this case are formed by the burning a mixture of hydrogen and the sample gas in the FID. The ions and electrons formed pass between an electrode gap and decrease the gap resistance. The resulting voltage drop is amplified by an electrometer and passed to a Hewlett-Packard Model 3390A integrator. When no effluent gas is flowing, a carrier gas (nitrogen) flows through the FID. Due to certain impurities in the carrier, some ions and electrons are formed creating a background voltage or zero shift. When the effluent gas enters the FID, the voltage increase above this zero shift is proportional to the degree of ionization or correspondingly the amount of tracer gas present. Since the chromatograph used in this study features a temperature control on the flame and electrometer, there is very low drift of the zero shift. Even given any zero drift, the HP 3390A, which integrates the effluent peak, also subtracts out the zero drift.

The lower limit of measurement is imposed by the instrument sensitivity and the background concentration of tracer within the air in the wind tunnel. Background concentrations were measured and subtracted from all data quoted herein.

3.4.2 *Sampling System*

The tracer gas sampling system consists of a series of fifty 30 cc syringes mounted between two circular aluminum plates. A variable-speed motor raises a third plate, which lifts the plunger on all 50 syringes, simultaneously. Computer controlled valves and tubing are connected such that airflow from each tunnel sampling point passes over the top of each designated syringe. When the syringe plunger is raised, a sample from the tunnel is drawn into the syringe container. The sampling procedure consists of flushing (taking and expending a sample) the syringe three times after which the test sample is captured. The draw rate is variable and generally set to be approximately 6 cc/min.

The sampling system was periodically calibrated to insure proper function of each of the valves and tubing assemblies. To calibrate the sampler each intake was connected to a manifold. The manifold, in turn, was connected to a gas cylinder having a known concentration of tracer gas. The gas was turned on, and a valve on the manifold was opened to release the pressure produced in the manifold. The manifold was allowed to flush for about one minute. Normal sampling procedures were carried out during calibration to insure exactly the same procedure is reproduced as when taking a sample from the tunnel. Each sample was then analyzed for tracer gas concentration. Percent error was calculated, and "bad" syringe/tube systems (error > 2 percent) were repaired or not used.

3.4.3 *Test Procedure*

The test procedure consisted of:

1) Setting the proper tunnel wind speed,
2) Releasing the metered mixtures of source gas from the plant stack,
3) Withdrawing samples of air from the tunnel designated locations, and
4) Analyzing the samples with a FID.

The samples were drawn into each syringe over a 200 s (approximate) time period and then consecutively injected into the GC.

The procedure for analyzing the samples from the tunnel is:

1) Introduce the sample into the GC which separates the ethane tracer gas from other hydrocarbons,
2) The voltage output from the chromatograph FID electrometer is sent to the HP 3390A Integrator,
3) the HP 3390A communicates the measured concentration in ppm to an IBM computer for storage, and

4) These values, χ_{mea}, along with the response levels for the background χ_{bg} and source χ_{source} are converted into source normalized model concentration by the equation:

$$\chi_m = \frac{\chi_{mea} - \chi_{bg}}{\chi_{source} - \chi_{bg}}$$

5) Field equivalent concentration values are related to model values by the equation:

$$\chi_p = \frac{\chi_m}{\chi_m + (1-\chi_m)[(\frac{T_a}{T_s})V]_m/[(\frac{T_a}{T_s})V]_p}, \quad \text{where } V = Q/U_H L^2,$$

and L is the characteristic length scale. When there is no distortion in the model-field volume flux ratio, V, and the plumes are isothermal this equation reduces to $\chi_p = \chi_m$.

Error Statement

Finite background concentrations, χ_{bg}, resulted from previous tests within the laboratory, these low levels could be measured to accuracies of 20 percent. The larger measured concentrations, χ_{mea}, were accurate to 2 percent. The source gas concentration, χ_{source}, was known to within 10 percent. Thus the source normalized concentration for $\chi_{mea} >> \chi_{bg}$ was accurate to approximately 10 percent. For low concentration values, $\chi_{mea} > \chi_{bg}$, the errors are larger.

4 TEST PROGRAM AND DATA FOR UCHSC VENTILATION STUDY

A physical modeling study of the UCHSC vent buildings was performed to assist in predicting environmental impacts for several proposed stack-building configurations. This involved:

1) The 1:150 reduced scale construction of all buildings within 900 feet of the School of Medicine site,
2) The placement of this model into a wind tunnel facility with the appropriate upwind roughness for this site,
3) Acquisition of velocity and turbulence profiles approaching and at the modeled UCHSC site,
4) Video taping of six different model plume for 16 different wind directions, and
5) Concentration measurements at either 48 (for the School of Medicine) or 34 (for the Biomedical Research Center) different sampling locations for two wind speeds and eight wind directions,

The following sub-sections discuss these topics in greater detail.

4.1 Model Construction

Based on atmospheric data over the UCHSC area, the size of the concentration grid, and modeling constraints discussed in Section 2 and the Appendix, a model scale of 1:150 was selected. Since the Environmental Wind Tunnel (see Figure 2) had a 12 foot turntable this allowed for the reduced scale construction of all significant buildings within a 900 foot radius of the UCHSC site. The location of the School of Medicine along with a circle demarking the portion of the Denver area which was replicated is shown in Figure 5.

The buildings surrounding the vent structures were fabricated from styrafoam and were covered on the top with masonite to make them solid and last longer for future display, and they were placed in their appropriate locations on a 12 foot diameter 1/4 inch masonite sheet. All roads and waterways were painted on this masonite sheet. The topography changes were modeled by layering the appropriate number of 1/4 inch sheets to match the land contours within the modeled area. Figure 5 shows the schematic picture of the entire 12 foot turntable model. The terrain upwind of the turntable area was modeled with a generic one inch roughness.

Ventilator buildings were constructed from manonite to permit incoparation of large ventilator plenums and accurate placement of inlet and exhaust openings. The primary ventilator buildings are the Biomedical Research Center and the School of Medicine.

4.2 Velocity Profiles

The techniques employed in the acquisition of velocity profiles are discussed in Section 3.2. The site model was located on a turntable, thus it could be rotated to simulate the different wind directions. An

approach flow upwind of the turntable model, typical of a suburban environment, was created through the placement of vortex generators at the tunnel entrance followed by 30 feet of 1 inch cube roughness on the tunnel floor.

Table 1 presents the data for the profile. Figure 3 and Figure 4 display plots of the mean velocity and longitudinal turbulent intensity profiles. The height coordinate in these tables and figures has been normalized by a model reference height of 1 meter (equivalent field height of 492 feet); thus, to obtain actual field heights multiply the normalized value by 492. Since a neutral boundary layer's velocity is invariant with respect to wind speed the normalized profiles presented can be converted to any field velocity at a specific height by the appropriate multiplicative constant.

The approach mean velocity profile for a suburban roughness condition was regressed to find the best log-log and log-linear fit. The log-log regression produced a power law exponent, p, equal to 0.24; i.e. $U/U_r = (z/z_r)^p$. The log-linear regression ($U/u_* = 2.5\ln\{(z-d)/z_o\}$) found a best fit roughness length, z_o, of 0.35 meters (field scale) and a displacement thickness, d, of 1.88 meters. These values of the power law exponent and the roughness length are appropiate for the Denver suburban roughness condition.

4.3 Visualization Test Results

Techniques employed to obtain a visible plume are discussed in Section 3.3. In Table 2 the eight runs recorded show the visualization conditions for both the School of Medicine (SOM) and the Biomedical Research Center (BRC) studies. The wind velocity for all these tests was 1 m/s at 10 meters height approaching the modeled area. A low wind speed was chosen to permit clear visualization of plume motions; however, similar path lines will also be followed by smoke particles at higher velocities.

Documentation on video cassettes of all visual tests have been provided to the sponsor prior to this report. If given a field to model wind speed ratio of 5 (= [5 m/s]/[1 m/s]) and a model to field length scale ratio of 150, then the time scale ratio between the model and the field is 1:30. Thus phenomena observed over the model in the wind tunnel will occur 30 times faster than observed at full scale. If the TV tapes were replayed in slow motion (30 times slower than the recorded speed), the observed plume trajectories and motions would appear realistic.

4.4 Concentration Data Results

Techniques employed to obtain the concentration data are discussed in Section 3.4.2. Figure 6 and Figure 7 show all the concentration sampling locations marked on a map of the modeled area. The first figure is for the School of Medicine and the second is for the Biomedical Research Center. Figure 8 shows a schematic of the manner simulant stack gases were introduced into the wind tunnel and subsequently sampled for

concentration analysis. Table 3 summarize the concentration test conditions for all 16 runs performed (once for the school of Medicine and once for the Biomedical Research Center). The field and model wind speeds indicated in this table were at equivalent heights of 10 meters.

Table 4 to Table 11 present the normalized concentration data, $\chi U_H/Q$, for all tests. This normalized concentration has units of m^{-2}. This normalized format is convenient because the concentration results, χ, from a test at one particular combination of wind speed, U_H, and flow rate, Q, can be extrapolated to other U_H, Q values provided that the ratio, U_H/Q, remains the same. Note that U_H is the wind speed at 10 meters height approaching the model area and not the value of wind speed above the vent site. The total flow rate, Q, out of the stacks is the exit velocity for a particular run times the total stack exit area.

5 DISCUSSION AND RECOMMENDATIONS

Selection of the final intake and exhaust stack configuration for the UCHSC site will be based upon the consideration of its visual appearance, zoning regulations, and minimization of environmental impact. The environmental effects of exhaust from the ventilator stacks will depend upon traffic volume, ventilator flow rates, state and federal ambient air-quality regulations, building and plume aerodynamics, and local meteorology. This study evaluates through fluid modeling the influence of building and plume aerodynamics on plume dilution. Data is reported in terms of normalized concentrations, K, where

$$K = \chi U/Q,$$

to permit concentration estimates for alternative traffic, exhaust and wind speed conditions. Concentrations can be estimated for alternative configurations, but acceptability must depend upon current air-quality standards.

The following discussion will focus upon evidence for reliability and consistency within the data set and advantages or disadvantages of different intake and stack configurations.

5.1 Smoke Visualization Results

A total of 19 smoke test cases were performed to evaluate the relative dispersion that occurs for various wind orientations, in which eight of those were completed for the School of Medicine (SOM) and the next eleven were for the Biomedical Research Center (BRC).

5.1.1 *School of Medicine*

The emissions from the Research Bridge and Hospital roofs, a highly toxic gas from a stack on the hospital (ETO), and fumes from a stack on the SOM roof (EF-91) were all simulated. Additionally the intakes on the Hospital roof, on the roof of the SOM, and on the SE annex of the SOM were also modeled.

The tests were conducted for a progressive series of the eight major compass points to evaluate the effects of various wind approach angles. As the air flow interacted with upwind buildings and their exhausts or intakes the plume trajectory was modified by the variation in streamline patterns.

Observations of visualization tests were performed to note the presence or absence of phenomena, such as

* Building downwash - Suction of a plume downward behind a structure or into a building cavity.

* Plume descent - Deflection of a plume groundward over a building cavity or slightly downwind of a structure.

* Vortices - Suction of a plume to the side or upwind into a building cavity or in the downwind region of a structure.

Conclusions from the smoke visualization tests

Major conclusions drawn from observations of the visualization tests are as follows:

1. Emissions from the Research Bridge and Hospital roof top tend to disperse and form a large plume which engulfs everything downwind of the Bridge. The fumes also tend to swirl about near the Hospital roof intakes.

2. Emissions from the stack on the SOM roof top do not appear to have much impact on the SOM itself. However, with a easterly wind there is some downwash into the larger of the two roof airhandler courtyards on the SOM. Some building downwash is also evident with a NE wind into the courtyard on the southern side of the SOM.

3. While there is often a large quantity of smoke at roof top levels for most of the structures grouped around the SOM, there does not appear to be a large amount of smoke which reaches ground level.

4. Even for a NW wind, which propels fumes from the SOM, Research Bridge and Hospital directly over the SE annex of the SOM; the smoke appears to be fairly well diffused in the vicinity of the intake on the east wall of the annex.

5. The highly toxic emissions from the stack on the Hospital (ETO) has such a small flow rate that, although it was modeled, its emissions can not be clearly discerned, consequently, no comment could be formulated with regard to this exhaust source and its effect upon the SOM and campus at large.

5.1.2 *Biomedical Research Center*

The emission from the Research Bridge roof tops, the emission from the BRC roof top, and the traffic from the Colorado Boulevard were evaluated. There are eight tests which were conducted similar to the SOM tests, but three additional tests were taped for a better visualization angles. The observations were also divided into building downwash, plume descent and vortices situations.

Conclusions from the smoke visualization tests

The major conclusions from the visualization test:

1. Emissions from the Research Bridge roof top tend to completely engulf any region downwind. Consequently there could be a considerable collection of pollutants from this source which may accumulate in regions where the air stagnates. The Plaza to the SE of the BRC being one such example.

2. There is some downwash of the exhaust vented from the BRC into the adjoining courtyard, especially for N,NW and SW wind directions. However, for the most part the fumes do not appear to have a strong effect upon the proposed BRC itself.

3. Vehicle emissions from Colorado Boulevard did have a considerable effect on the BRC. With wind coming from the N, the eddy in the wake of the BRC tends to draw the pollutants back into the BRC's SE courtyard. For winds coming from the NE, E, and SE directions, the auto emissions tend to impinge on the BRC, concentrating along its west and north sides, that would result in high concentration on the intakes proposed for the west side of the building. But with winds coming from the SW and W directions, the vortices caused by the obstacle of the BRC building tends to sweep the traffic exhaust westward or away from the building, that would cause low concentration at the proposed intake locations.

5.2 Influence of Wind Direction on Concentrations

By maintaining flow similarity between model and field conditions, relative concentrations (χ/Q) for a given source configuration, building configuration and wind direction will be invariant. The wind tunnel relative concentration measurements for the UCHSC building complex will be the same as those that could be obtained during full-scale measurements under the same ambient conditions.

Variation of wind orientation produces a wide variance in sample concentrations.

5.2.1 *School of Medicine*

Figure 9 shows concentrations measured at all the sampling locations from the three exhaust sources for the NE wind direction. Because the ETO stack is close to the intakes on the Hospital roof top and the exit velocity for the stack is large, the Maximum K concentration reaches a value as high as 6,000. Figure 10 to Figure 12 show concentration levels for all the sampling locations for four major wind directions. Concentrations at the intakes on the Hospital roof top are always higher than the other locations sampled.

5.2.2 *Biomedical Research Center*

Figure 13 to Figure 15 indicate concentrations measured at the sampling points #4, #19 and #26 under different wind directions for each

exhaust source. Sampling point #19 detects the highest K concentration value measured during the entire test (13,000 from the traffic exhaust). This indicates that the traffic exhaust strongly effects the proposed intake locations. This conclusion is also supported by Figure 16 and Figure 17. The wind coming from the E produces 20 times higher K coefficient than the wind coming from the west. This phenomenon was also shown during the visualization program. Figure 18 to Figure 20 demonstrate sampling point behavior for the four major wind directions and each individual source.

5.3 RECOMMENDATIONS

Based on the concentration data acquired during this study, there are two recommendations as follows:

1. The intakes on the Hospital roof top should be closed and removed in order to avoid the highly hazardous ETO stack.

2. The best location for the potential intakes at the Biomedical Research Center should be on the roof top near the sampling point # 4 of that building to avoid the traffic exhaust.

REFERENCES

Allwine, K. J., Meroney, R. N., and Peterka, J. A. (1978), "Rancho Seco Building Wake Effects on Atmospheric Diffusion: Simulation in a Meteorological Wind Tunnel," FDDL Report No. CER77-78KJA-RNM-JAP25, Colorado State University, Fort Collins, Colorado.

Arya, S. P. S., and Plate, E. J. (1969), "Modeling of the Stably Stratified Atmospheric Boundary Layer," J. Atmos. Sci., Vol. 26, No. 4, pp. 656-665.

Ayra, S. P. S. (1975), "Buoyancy Effects in a Horizontal Flat-Plate Boundary Layer," J. Fluid Mech., Vol. 68, Pt. 2, pp. 321-343.

Barad, M. L., Ed. (1958), Project Prairie Grass: A Field Program in Diffusion, Geophysical Research Papers, No. 59, Vols. I and II, Report AFCRC-TR-58-235, Air Force Cambridge Research Center.

Brunn, (1978), "Multi-Probes and Higher Moments," Proceedings of the Dynamic Flow Conference 1978, pp. 943-961.

Cermak, J. E. (1975), "Applications of Fluid Mechanics to Wind Engineering--A Freeman Scholar Lecture," J. of Fluids Engineering, Vol. 97, pp. 9-38.

Cermak, J. E., Shrivastava, P. K., and Poreh, M. (1983), "wind-tunnel Research on the Mechanics of Plumes in the Atmospheric Surface Layer," Civil Engineering Department Report CER83-84JEC-PKS-MP12, Colorado State University, Fort Collins, CO, Annual Progress Report to U.S. Dept. of Army Contract DAAK11-82-K-0004, 140 pp.

Chaudhry, F. H. and Meroney, R. N. (1973), "A Laboratory Study of Diffusion in Stably Stratified Flow," Atmos. Envir., Vol. 7, pp. 443-454. Chien, H. C., Meroney, R. N., and Sandborn, V. A. (1979), "Sites for Wind-Power Installations: Physical Modeling of the Wind Field Over Kahuku Point, Hawaii," FDDL Report No. CER79-80HCC-RNM-VAS25, Colorado State University, Fort Collins, Colorado.

Counihan, J. (1975), "Adiabatic Atmospheric Boundary Layers: A Review and Analysis of Data from the Period 1880-1972," Atmos. Envir., Vol. 9, pp. 871-905.

Fage, A. and Warsap, J. H. (1929), "Effects of Turbulence and Surface Roughness on Drag of Circular Cylinders," U.K., ARC R&M 1283.

Farell, C., Carrasquel, S., Guven, O., and Patel, V. C. (1977), "Effect of Wind-Tunnel Walls on the Flow Past Circular Cylinders and Cooling Tower Models," J. of Fluids Engineering, Vol. 99, pp. 470-479.

Gifford, F. A. (1976), Turbulent Diffusion-Typing Schemes: A Review, Nucl. Saf., Vol. 17, No. 1, pp. 72 ff.

Golden, J. (1961), "Scale Model Techniques," M.S. Thesis, Dept. of Met. and Ocean., New York University, 42 pp.

Golder, D. G. (1972), "Relations Among Stability Parameters in the Surface Layer," Boundary-Layer Meteorol., Vol. 3, No. 1, pp. 47-58.

Halitsky, J., Colden, J., Halpern, P., and Wu, P. (1963), "Wind Tunnel Tests of Gas Diffusion from a Leak in the Shell of a Nuclear Power Reactor and from a Nearby Stack," N.Y.U. Meteorol. and Oceanog. Geophys. Sciences Lab. Report 63-2 (New York Univ., College of Engineering, New York.)

Halitsky, J. (1968), "Gas Diffusion Near Buildings," Meteorology and Atomic Energy, 1968, editor D. H. Slade, Atomic Energy Commission, Ch. 5-5, pp. 221-256.

Hatcher, R. V. and Meroney, R. N. (1977), "Dispersion in the Wake of a Model Industrial Complex," Joint Conf. on Applications of Air Pollution Meteorology, Proceedings, Am. Meteorol. Sco., Salt Lake City, Utah, 29 November - 2 December, 1977, pp. 343-346.

Haugen, D. A., Kaimal, J. C., and Bradley, E. F. (1971), "an Experimental Study of Reynolds Stress and Heat Flux in the Atmospheric Surface Layer," Quart. J. Roy. Meteorol. Soc., Vol. 97, pp. 168-180.

Hinze, J. O. (1975), Turbulence, McGraw-Hill, New York, 2nd. edition, 790 pp.

Horst, T. W. (1979), "Lagrangian Similarity Modeling of Vertical Diffusion from a Ground Level Source," J. Appl. Meteorol., Vol. 18, pp. 733-740.

Hosker, R. P., Jr. (1984), "Flow and Diffusion Near Obstacles," Atmospheric Science and Power Production, DOE/TIC-27601, pp. 241-326.

Hsi, G., and Cermak, J. E. (1965), "Meteorological-Tower Induced Wind Field Perturbations," Prepared under U.S. Army Research Grant DA-AMC-28-043-64-G-9, Fluid Mechanics Program Report No. CER65GH-JEC49, Colorado State University, Fort Collins, Colorado.

Hunt, J. C. R. (1974), "Wakes Behind Buildings," presented at the Aeronautical Research Council's Atmospheric Environment Committee Meeting, Oct. 23, ARC Report 35601, Atmos. 229, Aeronautical Research Council of Great Britain, Her Majesty's Stationery Office, London.

Hunt, J. C. R., Snyder, W. H., and Lawson, F. E., Jr. (1978), "Flow Structure and Turbulent Diffusion around a Three-Dimensional Hill: Fluid Modeling Study on Effects of Statification: Part I: Flow Structure," Envir. Prot. Agcy. Report No. EPA 600/4-78-041, Fesearch Triangle Park, NC, 84 pp.

Islitzer, N. F. and Dumbauld, R. K. (1963), "Atmospheric Diffusion Deposition Studies over Flat Terrain," INt. J. Air Water Pollut., Vol. 7 (11-12), pp. 999-1022.

Kline, S. J. (1965), Similitude and Approximation Theory, McGraw-Hill Book Company, New York, 229 pp.

Kothari, K. M., Meroney, R. N., Bouwmeester, (1981), "An Algorithm to Estimate Field Concentrations Under Nonsteady Meteorological Conditions from Wind Tunnel Experiments," Jornal of Applied Meteorology, Vol. 30, pp. 92-101.

Kothari, K. M., Meroney, R. N. and Peterka, J. A. (1979), "Nuclear Power Plant Building Works Effects on Atmosphere Diffusion," EPRI Report No. 1891, CER79-80KMK-RNM-JAP28, 109 pp.

Lamb, R. G. (1982), "Diffusion in the Convective Boundary Layer," Chapter 5, Atmospheric Turbulence and Air Pollution Modeling, Nieuwstadt and van Dop, editors, D. Reidel Publishing Company, Dordrecht, Holland, pp. 159-230.

Meroney, R. N. (1980), "Wind-Tunnel Simulations of the Flow Over Hills and Complex Terrain," J. of Industrial Aerodynamics, Vol. 5, pp. 297-321.

Meroney, R. N. (1982), "Turbulent Diffusion Near Buildings," Engineering Meteorology, Chapter 11, pp. 481-521.

Meroney, R. N., Cermak, J. E., and Garrison, J. A. (1975a), "Wind-Tunnel Study of Stack Gas Dispersal at Lansing Power Station, Units 1, 2, 3, and 4," FDDL Report No. CER74-75RNM-JEC-JAG28, Colorado State University, Fort Collins, Colorado.

Meroney, R. N., Cermak, J. E., and Garrison, J. A. (1975b), "Wind-Tunnel Study of Stack Gas Dispersal at Lansing Power Station, Units 1, 2, 3, and 4," FDDL Report No. CER74-75RNM-JEC-JAG29, Colorado State University, Fort Collins, Colorado.

Meroney, R. N., Sandborn, V. A., Bouwmeester, R. J. B., Chien, H. C., and Rider, M. (1978), "Sites for Wind-Power Installations: Physical Modeling of the Influence of Hills, Ridges and Complex Terrain - Part II: Executive Summary," Dept. of Energy Report RLO/2438-77/3, 90 pp.

Neff, D. E., Tan T. Z., and Meroney, R. N. (1988), "Fluid Modeling of Exhaust Gas Dispersion from the Parcel 7 Ventilation Site, Central Artery/Third Harbor Tunnel Project," FDDL Report No. CER88-DEN-RNM-6, Colorado State University, Fort Collins, Colorado.

Niemann, H. J. and Ruhwedel, J. (1980), "Full-scale and Model Tests on Wind-induced, Static and Dynamic Stresses in Cooling Tower Shells," Eng. Struct., Vol. 2, pp. 81-89.

Ogawa, Y., Diosey, P. G., Uehara, K., and Ueda, H. (1985), "Wind Tunnel Observation of Flow and Diffusion Under Stable Stratification," Atmos. Envir., Vol. 19, pp. 65-74.

Peterka, J. A., Meroney, R. N. and Kothari, K. (1985), "Wind Flow Patterns About Buildings," J. of Wind Engineering and Industrial Aerodynamics, Vol. 21, pp. 21-38.

Plate, E. J. and Cermak, J. E. (1963), "Micro-meteorological Wind-Tunnel Facility," Fluid Dynamics and Diffusion Laboratory Report CER63EJP-JEC9, Colorado State University, Fort Collins, Colorado, 65 pp.

Poreh, M. and Cermak, J. E. (1984), "Wind Tunnel Research on the Mechanics of Plumes in the Atmospheric Surface Layer, Part II," Annual Report to U.S. Dept. of Army, Chemical Systems Laboratory, Aberdeen Proving Ground, Maryland, Colorado State University Civil Engineering Department Report CER84-85MP-JEC47, 45 pp.

Fanga Raju, K. G. and Singh, V. (1976), "Blockage Effects on Drag of Sharp Edged Bodies," J. of Industrial Aerodynamics, Vol. 1, pp. 301-309.

Schlichting, H. (1968), Boundary Layer Theory, McGraw-Hill Book Company, New York, 774 pp.

Schon, J. P. and Mery, P. (1971), "A Preliminary Study of the Simulation of Neutral Atmospheric Boundary Layer Using Air Injection in a Wind Tunnel," Atmos. Enviro., Vol. 5, No. 5, pp. 299-312.

Sethurama, S., and Cermak, J. E. (1973), "Stratified Shear Flows Over a Simulated Three-Dimensional Urban Heat Island," Project Themis Technical Report No. 23, CER73-74SS-JEC4, Colorado State University, Fort Collins, Colorado.

Snyder, W. H., Britter, R. E., and Hunt, J. C. R. (1979), "A Fluid Modeling Study of the Flow Structure and Plume Impingement on a Three-Dimensional Hil in Stably Stratified Flow," Proc. Fifth Int. Conf. on Wind Engr., Pergamon Press, NY, Vol. 1, pp. 319-329.

Snyder, W. H. (1981), "Guidelines for Fluid Modeling of Atmospheric Diffusion," EPA Report EPA-600/8-81-009, 185 pp.

Szechenyi, E. (1975), "Supercritical Reynolds Number Simulation for Two dimensional Flow over Circular Cylinders," J. Fluid Mech., Vol. 70, pp. 529-542.

Teunissen, H. W. (1975), "Simulation of the Planetary Boundary Layer in a Multiple Jet Wind Tunnel," Atmos. Envir., Vol. 9, pp. 145-174.

Willis, G. E. and Deardorff, J. W. (1974), "A Laboratory Model of the Unstable Planetary Boundary Layer," J. Atmos. Sci., Vol. 31, pp. 1297-1307.

Willis, G. E. and Deardorff, J. W. (1976), "A Laboratory Model of Diffusion into the Convective Planetary Boundary Layer," Quart. J. Roy. Meteorol. Soc., Vol. 102, pp. 427-445.

Willis, G. E. and Deardorff, J. W. (1978), "A Laboratory Study of Dispersion from an Elevated Source Within a Modeled Convective Planetary Boundary Layer," Atmos. Envir., Vol. 12, pp. 1305-1311.

Yamada, T. and Meroney, R. N. (1971). "Numerical and Wind-Tunnel Simulation of Response of Stratified Shear Layers to Nonhomogeneous Surface Features," CER7071TY-RNM62, Colorado State University, also (AD-730-953).

TABLES

Table 1 Data for Velocity and Turbulence Profiles

Type profile 0>volt, 1>wire, 2>x-wire, 4>pitot = 1
Number of profiles in the file = 1
Number of points per profile = 18
Units of Height = cm
Units of Velocity = m/s

Normalized Height	Normalized Velocity	Turbulence Intensity
0.02	0.23	45.23
0.03	0.31	43.92
0.04	0.39	38.83
0.04	0.40	33.63
0.06	0.50	28.24
0.08	0.59	25.01
0.12	0.68	20.66
0.16	0.75	16.37
0.20	0.79	14.96
0.30	0.81	10.18
0.40	0.89	8.78
0.50	0.93	6.33
0.60	0.96	5.68
0.70	0.97	5.01
0.80	0.98	4.57
0.90	0.99	4.76
1.00	1.00	5.06
1.10	1.03	5.43

Table 2 Visualization Test Plan

Run #	Speed (m/s)	WT Setting	WD
1	1.0	825	N
2	1.0	825	NE
3	1.0	825	E
4	1.0	825	SE
5	1.0	825	S
6	1.0	825	SW
7	1.0	825	W
8	1.0	825	NW

Table 3 Concentration Test Plan

Run #	Full Scale Speed (m/s)	WT Speed (m/s)	WT Setting	WD
1	4.4	2.2	1675	N
2	4.4	2.2	1675	NE
3	4.4	2.2	1675	E
4	4.4	2.2	1675	SE
5	4.4	2.2	1675	S
6	4.4	2.2	1675	SW
7	4.4	2.2	1675	W
8	4.4	2.2	1675	NW
9	8.8	4.4	3200	N
10	8.8	4.4	3200	NE
11	8.8	4.4	3200	E
12	8.8	4.4	3200	SE
13	8.8	4.4	3200	S
14	8.8	4.4	3200	SW
15	8.8	4.4	3200	W
16	8.8	4.4	3200	NW

Table 4 Concentration Results I (SOM)

Point No.	X (ft)	Y (ft)	Z (ft)	Run No. 1 K S1	Run No. 1 K S2	Run No. 1 K S3	Run No. 2 K S1	Run No. 2 K S2	Run No. 2 K S3	Run No. 3 K S1	Run No. 3 K S2	Run No. 3 K S3	Run No. 4 K S1	Run No. 4 K S2	Run No. 4 K S3
1	0	-75	5	34	335	64	1	246	0	0	5	0	1	6	0
2	0	-68.75	57.5	98	1071	185	5	515	0	0	5	0	0	2	0
3	0	0	78.75	149	330	266	1	27	0	0	1110	0	0	36	0
4	45	3.75	57.5	136	374	232	1	39	0	0	161	0	0	110	6
5	-15	7.5	58.75	147	317	307	1	21	6	0	1823	6	0	50	12
6	-50	7.5	58.75	148	315	371	3	17	12	0	2418	0	0	26	6
7	108.75	10	5	56	125	98	1	0	6	0	8	6	1	3	6
8	0	47.5	78.75	131	279	249	1	11	6	0	5	6	0	966	12
9	0	92.5	5	70	156	127	2	14	6	0	3	6	1	26	6
10	-95	143.75	57.5	116	249	411	1240	2611	1887	10	120	41	1	1661	12
11	-188.75	215	70	26	63	127	696	1460	1123	355	808	562	3	1063	29
12	-247.5	-10	5	11	32	41	439	921	753	2	812	17	1	23	17
13	-151.25	-137.5	46.25	55	123	168	26	502	69	0	11	17	0	3	12
14	65	155	5	23	56	64	3	12	17	0	2	12	1	3	12
15	218.75	267.5	5	2	15	6	0	0	6	0	2	6	1	5	17
16	151.25	142.5	43.75	37	86	64	1	9	0	0	2	6	0	2	12
17	78.75	-160	62.5	84	559	151	1	15	12	0	2	17	0	3	12
18	151.25	-43.75	57.5	48	108	93	1	9	12	0	2	12	0	2	29
19	136.25	-101.25	45	21	51	46	0	9	12	0	0	17	0	2	23
20	97.5	81.25	46.25	81	177	151	1	11	6	0	2	6	0	2	12
21	-171.25	518.75	31.25	0	11	17	19	45	41	25	53	58	1067	2392	2223
22	65	511.25	113.75	125	266	261	767	1595	1146	1004	2077	1505	759	1583	1158
23	25	511.25	113.75	43	96	191	134	281	220	247	509	382	251	518	405
24	-63.75	511.25	113.75	675	1407	2999	1012	2120	5969	718	1509	1609	1227	2590	2692
25	-87.5	511.25	113.75	656	1368	3694	932	1946	3844	603	1281	1801	1121	2365	2733
26	-68.75	532.5	113.75	75	164	301	96	206	533	194	405	481	324	692	683
27	32.5	532.5	113.75	11	32	58	44	96	98	93	189	162	108	222	203
28	73.75	532.5	113.75	53	125	110	117	260	197	268	580	452	265	574	440
29	62.5	526.25	115	22	53	64	4	15	12	71	147	116	155	324	249
30	-401.25	240	-2.5	0	9	6	29	66	52	45	93	116	282	1041	585
31	-2.5	235	12.5	41	93	174	4	17	17	0	2	12	2	8	17
32	-2.5	275	12.5	35	80	133	5	18	17	0	2	6	1	2	17
33	-2.5	315	12.5	21	53	87	5	18	12	0	3	12	1	5	17
34	-2.5	353.75	12.5	44	101	185	15	38	29	3	8	17	3	6	17
35	-2.5	405	12.5	61	134	301	18	45	35	0	2	12	1	3	17
36	-60	-171.25	57.5	136	527	324	2	1209	12	0	15	12	1	6	17
37	-92.5	638.75	5	0	11	6	2	14	0	6	14	12	77	161	145
38	256.25	800	3.75	0	11	12	0	0	6	0	0	6	1	3	17
39	637.5	535	87.5	0	9	6	0	0	6	0	0	12	0	2	23
40	381.25	225	32.5	0	9	0	0	0	0	0	0	6	0	2	17
41	525	83.75	37.5	0	9	12	0	0	6	0	0	6	1	3	17
42	410	81.25	0	0	9	6	1	0	6	0	0	6	0	2	17
43	441.25	-228.75	31.25	0	9	12	1	0	6	0	0	6	0	2	12
44	437.5	-228.75	31.25	0	9	6	0	0	6	0	0	12	0	2	17
45	590	-297.5	15	0	9	0	1	0	6	0	0	12	0	2	17
46	-213.75	180	73.75	1	11	0	285	601	619	133	345	226	2	105	23
47	-413.75	247.5	10	0	9	6	432	909	805	267	862	498	72	243	203
48	-292.5	115	-1.25	10	30	41	400	838	695	11	518	35	1	29	35

Table 5 Concentration Results II (SOM)

Point No.	X (ft)	Y (ft)	Z (ft)	Run No. 5 K S1	Run No. 5 K S2	Run No. 5 K S3	Run No. 6 K S1	Run No. 6 K S2	Run No. 6 K S3	Run No. 7 K S1	Run No. 7 K S2	Run No. 7 K S3	Run No. 8 K S1	Run No. 8 K S2	Run No. 8 K S3
1	0	-75	5	0	2	0	0	2	0	0	9	0	2	17	0
2	0	-68.75	57.5	0	2	0	0	2	0	0	9	0	4	86	6
3	0	0	78.75	0	3	0	0	3	0	0	9	6	5	18	12
4	45	3.75	57.5	0	18	6	0	219	0	0	14	6	61	266	122
5	-15	7.5	58.75	0	3	0	0	3	0	0	9	6	2	14	12
6	-50	7.5	58.75	0	5	0	0	3	0	0	11	6	1	0	6
7	108.75	10	5	0	2	0	0	56	0	0	336	6	319	901	608
8	0	47.5	78.75	0	9	0	0	3	0	0	11	6	7	23	23
9	0	92.5	5	0	209	0	0	5	41	0	11	12	68	152	145
10	-95	143.75	57.5	0	21	0	0	5	12	0	11	12	1	0	12
11	-188.75	215	70	128	300	336	1	6	12	0	11	12	1	0	12
12	-247.5	-10	5	0	5	17	0	3	0	0	9	12	1	0	6
13	-151.25	-137.5	46.25	0	2	6	0	2	6	0	0	6	0	0	12
14	65	155	5	9	357	12	1	8	46	3	15	17	46	107	116
15	218.75	267.5	5	23	668	46	80	182	1285	100	261	278	456	955	886
16	151.25	142.5	43.75	0	30	0	3	278	17	235	499	365	739	1550	1389
17	78.75	-160	62.5	0	2	0	0	2	6	1	11	23	6	101	23
18	151.25	-43.75	57.5	0	2	6	0	6	0	0	93	17	170	2018	330
19	136.25	-101.25	45	0	2	6	0	5	6	0	51	12	397	957	758
20	97.5	81.25	46.25	0	53	0	0	1012	12	1	33	12	440	1018	822
21	-171.25	518.75	31.25	568	1273	1279	2	20	29	1	14	17	2	14	17
22	65	511.25	113.75	186	1059	318	351	746	619	340	725	1320	296	626	689
23	25	511.25	113.75	225	1131	371	163	348	289	178	381	1216	214	454	596
24	-63.75	511.25	113.75	1550	3509	2437	513	1096	828	614	1296	1059	777	1632	1361
25	-87.5	511.25	113.75	1252	2772	2032	234	508	399	335	712	562	432	912	718
26	-68.75	532.5	113.75	672	1560	1181	722	1523	1117	341	731	567	362	778	602
27	32.5	532.5	113.75	225	863	417	363	761	579	320	676	718	55	125	168
28	73.75	532.5	113.75	290	1102	486	360	775	683	354	752	851	123	282	307
29	62.5	526.25	115	59	835	104	300	640	544	282	598	1083	157	338	417
30	-401.25	240	-2.5	36	93	104	1	6	23	1	12	23	1	9	12
31	-2.5	235	12.5	35	707	64	1	11	394	0	11	35	0	0	64
32	-2.5	275	12.5	85	979	174	1	14	434	0	12	41	1	0	122
33	-2.5	315	12.5	151	1152	336	1	17	457	1	14	35	1	12	104
34	-2.5	353.75	12.5	292	1389	666	2	20	1870	6	24	208	8	26	359
35	-2.5	405	12.5	233	1255	538	2	17	4307	0	12	915	1	11	677
36	-60	-171.25	57.5	1	8	6	0	3	12	0	11	12	0	0	12
37	-92.5	638.75	5	378	842	811	5	20	23	0	12	12	0	0	12
38	256.25	800	3.75	3	96	6	206	470	469	1	15	23	0	9	12
39	637.5	535	87.5	0	0	6	4	233	12	58	131	174	1	9	12
40	381.25	225	32.5	0	2	0	0	131	6	220	574	359	134	290	289
41	525	83.75	37.5	0	0	0	0	2	0	36	542	64	109	240	237
42	410	81.25	0	0	0	0	0	8	6	23	839	46	245	524	498
43	441.25	-228.75	31.25	0	0	0	0	2	0	0	99	12	271	571	544
44	437.5	-228.75	31.25	0	0	0	0	2	0	0	9	6	279	688	544
45	590	-297.5	15	0	0	0	0	0	0	0	0	12	221	514	440
46	-213.75	180	73.75	1	8	12	0	3	6	0	11	6	1	9	17
47	-413.75	247.5	10	2	12	12	0	5	12	0	11	12	1	0	12
48	-292.5	115	-1.25	0	5	6	0	3	6	0	11	12	0	9	12

Table 6 Concentration Results III (SOM)

Point No.	X (ft)	Y (ft)	Z (ft)	Run No. 9 S1	Run No. 9 K S2	Run No. 9 S3	Run No. 10 S1	Run No. 10 K S2	Run No. 10 S3	Run No. 11 S1	Run No. 11 K S2	Run No. 11 S3	Run No. 12 S1	Run No. 12 K S2	Run No. 12 S3
1	0	-75	5	92	1117	208	1	258	0	1	0	0	0	0	0
2	0	-68.75	57.5	122	1712	243	6	1042	0	1	18	0	0	0	0
3	0	0	78.75	159	345	301	1	27	0	0	1754	0	0	0	58
4	45	3.75	57.5	124	306	220	0	78	46	0	99	23	0	0	116
5	-15	7.5	58.75	159	348	336	7	39	347	0	2340	12	0	0	58
6	-50	7.5	58.75	161	348	405	12	51	58	0	2787	35	32	0	104
7	108.75	10	5	53	135	116	1	18	12	0	24	12	0	0	0
8	0	47.5	78.75	142	312	278	0	0	359	0	0	35	0	1343	69
9	0	92.5	5	71	165	139	2	18	23	1	0	12	0	0	46
10	-95	143.75	57.5	123	273	463	1377	2892	2107	12	174	58	53	2144	139
11	-188.75	215	70	21	60	162	671	1409	1123	376	874	602	0	814	0
12	-247.5	-10	5	9	36	46	442	931	776	3	904	35	0	0	0
13	-151.25	-137.5	46.25	60	141	197	38	550	104	0	24	23	0	0	0
14	65	155	5	24	66	127	2	21	347	0	0	12	0	0	0
15	218.75	267.5	5	6	39	46	0	18	58	1	0	23	0	0	0
16	151.25	142.5	43.75	37	111	104	1	21	35	1	0	12	0	0	0
17	78.75	-160	62.5	81	402	151	0	21	58	1	0	23	0	0	0
18	151.25	-43.75	57.5	48	153	104	1	24	35	0	18	58	0	0	0
19	136.25	-101.25	45	22	75	69	1	18	371	0	0	23	0	0	0
20	97.5	81.25	46.25	82	198	174	1	21	35	1	0	23	0	0	139
21	-171.25	518.75	31.25	1	21	23	16	51	104	24	63	81	1054	2183	2212
22	65	511.25	113.75	229	502	463	562	1189	880	1018	2123	1540	917	1751	1378
23	25	511.25	113.75	68	165	266	117	261	220	221	469	347	180	228	266
24	-63.75	511.25	113.75	1264	2676	3624	1175	2484	5396	1150	2424	1992	2029	4046	6959
25	-87.5	511.25	113.75	903	1910	3786	897	1889	3948	633	1340	1401	1879	3733	6866
26	-68.75	532.5	113.75	151	351	498	109	243	567	202	435	382	1064	2126	2038
27	32.5	532.5	113.75	22	66	104	36	90	116	95	207	185	178	225	255
28	73.75	532.5	113.75	90	219	197	99	228	220	225	490	382	246	384	394
29	62.5	526.25	115	37	105	139	3	27	58	70	159	127	3	0	0
30	-401.25	240	-2.5	0	18	12	118	255	243	48	114	127	199	802	475
31	-2.5	235	12.5	40	102	278	4	21	58	0	0	23	4	0	0
32	-2.5	275	12.5	37	96	266	4	24	58	0	0	23	0	0	0
33	-2.5	315	12.5	16	51	127	4	24	46	1	0	23	0	0	0
34	-2.5	353.75	12.5	51	123	278	22	63	93	5	24	46	0	0	0
35	-2.5	405	12.5	36	93	371	16	48	93	1	0	35	0	0	0
36	-60	-171.25	57.5	141	655	347	2	2159	46	0	45	104	0	0	0
37	-92.5	638.75	5	1	21	12	0	24	0	8	27	12	75	9	93
38	256.25	800	3.75	0	18	12	0	0	301	0	0	12	0	0	0
39	637.5	535	87.5	0	0	12	0	0	35	0	0	23	0	0	0
40	381.25	225	32.5	2	27	46	1	18	35	0	0	23	0	0	0
41	525	83.75	37.5	1	24	12	1	18	35	0	0	23	0	0	0
42	410	81.25	0	3	36	35	1	21	12	0	0	23	0	0	0
43	441.25	-228.75	31.25	3	33	35	1	15	23	0	0	23	0	0	0
44	437.5	-228.75	31.25	4	36	35	1	18	35	1	0	23	0	0	0
45	590	-297.5	15	3	30	35	1	15	35	1	0	35	0	0	0
46	-213.75	180	73.75	1	21	35	257	547	614	147	408	255	0	0	0
47	-413.75	247.5	10	1	21	23	380	805	811	322	844	672	112	339	405
48	-292.5	115	-1.25	9	36	46	395	835	706	11	667	46	0	0	0

Table 7 Concentration Results IV (SOM)

Point No.	X (ft)	Y (ft)	Z (ft)	Run No. 13 K S1	Run No. 13 K S2	Run No. 13 K S3	Run No. 14 K S1	Run No. 14 K S2	Run No. 14 K S3	Run No. 15 K S1	Run No. 15 K S2	Run No. 15 K S3	Run No. 16 K S1	Run No. 16 K S2	Run No. 16 K S3
1	0	-75	5	1	18	0	1	0	0	0	0	0	1	9	0
2	0	-68.75	57.5	0	0	0	1	0	0	0	0	0	3	129	0
3	0	0	78.75	0	0	0	0	15	0	0	0	0	5	9	0
4	45	3.75	57.5	0	39	0	0	345	0	0	18	0	34	168	46
5	-15	7.5	58.75	0	0	12	0	18	0	0	0	0	2	3	0
6	-50	7.5	58.75	0	0	0	0	15	0	0	0	0	0	0	0
7	108.75	10	5	0	0	12	0	99	0	0	1081	0	354	1337	648
8	0	47.5	78.75	0	27	0	0	18	0	0	0	0	6	15	0
9	0	92.5	5	1	360	0	1	21	58	0	0	0	102	219	162
10	-95	143.75	57.5	0	36	23	0	18	0	0	0	0	0	3	0
11	-188.75	215	70	136	327	347	1	18	12	0	0	0	0	0	0
12	-247.5	-10	5	0	0	12	0	0	23	0	0	0	0	0	0
13	-151.25	-137.5	46.25	0	0	12	0	0	0	0	0	0	0	0	0
14	65	155	5	19	553	23	2	24	23	2	0	0	54	117	104
15	218.75	267.5	5	45	784	81	102	246	1447	124	312	336	413	853	822
16	151.25	142.5	43.75	0	90	0	6	387	12	229	487	347	913	1889	1656
17	78.75	-160	62.5	0	0	0	0	0	0	1	0	0	4	39	0
18	151.25	-43.75	57.5	0	0	0	0	27	0	0	231	0	175	3481	289
19	136.25	-101.25	45	0	0	0	0	18	12	0	60	0	408	1009	753
20	97.5	81.25	46.25	0	192	23	0	2084	35	1	111	0	505	1309	903
21	-171.25	518.75	31.25	551	1234	1262	3	39	23	1	15	35	2	6	0
22	65	511.25	113.75	286	1240	475	381	817	637	341	718	1146	322	664	695
23	25	511.25	113.75	431	1520	672	150	336	255	142	306	926	170	351	509
24	-63.75	511.25	113.75	2160	4760	3335	667	1430	1065	1294	2688	1980	931	1931	1748
25	-87.5	511.25	113.75	1591	3475	2536	232	526	405	531	1111	822	457	949	868
26	-68.75	532.5	113.75	799	1811	1332	633	1340	973	257	553	405	324	673	521
27	32.5	532.5	113.75	286	1015	486	262	565	440	222	472	556	47	99	116
28	73.75	532.5	113.75	334	1189	556	350	763	637	279	592	602	99	213	197
29	62.5	526.25	115	89	871	162	247	538	452	208	442	811	142	291	405
30	-401.25	240	-2.5	40	114	104	1	21	0	1	0	0	1	3	0
31	-2.5	235	12.5	76	862	139	1	27	486	0	0	23	0	0	35
32	-2.5	275	12.5	162	1138	324	1	27	567	0	0	23	0	0	104
33	-2.5	315	12.5	259	1052	556	2	33	567	1	0	23	1	3	81
34	-2.5	353.75	12.5	485	1748	1077	3	36	2049	15	45	266	15	30	347
35	-2.5	405	12.5	393	1544	926	3	36	4134	0	0	1401	0	3	660
36	-60	-171.25	57.5	2	21	0	0	0	12	0	0	0	0	0	0
37	-92.5	638.75	5	363	814	799	6	33	23	0	0	0	0	0	0
38	256.25	800	3.75	5	105	35	217	499	486	1	0	23	0	0	0
39	637.5	535	87.5	0	15	12	5	237	0	57	129	162	0	0	0
40	381.25	225	32.5	0	18	12	0	126	0	260	649	394	109	225	243
41	525	83.75	37.5	0	0	12	0	0	0	29	631	46	107	225	232
42	410	81.25	0	0	0	12	0	21	0	23	1036	12	255	532	498
43	441.25	-228.75	31.25	0	0	12	0	0	0	0	72	0	298	619	579
44	437.5	-228.75	31.25	0	0	12	0	0	12	0	0	0	317	775	602
45	590	-297.5	15	0	0	35	0	0	0	0	0	0	244	568	452
46	-213.75	180	73.75	0	18	12	0	0	0	0	0	0	1	3	0
47	-413.75	247.5	10	3	30	35	0	18	23	0	0	12	0	0	0
48	-292.5	115	-1.25	0	0	0	0	0	0	0	0	0	0	0	0

Table 8 Concentration Results I (BRC)

1. Bridge exhaust = 76.27 cu m/s
2. BRC roof exhaust = 37.76 cu m/s
3. Traffic exhaust = 4.5 cu m/s

Wind speed = 4.4 m/s at 10 m for Run No.1 - 8.
Wind speed = 8.8 m/s at 10 m for Run No.9 - 16.

K = Conc * U / Q U: Wind Speed Q: Exhaust flow rate

Point No.	X (ft)	Y (ft)	Z (ft)	Run No. 1 S1	Run No. 1 K S2	Run No. 1 K S3	Run No. 2 S1	Run No. 2 K S2	Run No. 2 K S3	Run No. 3 S1	Run No. 3 K S2	Run No. 3 K S3	Run No. 4 S1	Run No. 4 K S2	Run No. 4 K S3
1	-367.5	-45	73.75	0	807	41	258	467	31	3	65	1	0	37	0
2	-367.5	105	73.75	0	43	27	227	1038	26	25	108	4	0	45	0
3	-350	162.5	73.75	0	42	64	214	154	26	109	543	20	0	24	0
4	-332.5	167.5	73.75	1	23	79	234	116	28	131	500	22	0	38	0
5	-213.75	180	73.75	0	11	30	210	57	24	161	656	29	0	32	0
6	-362.5	193.75	73.75	0	3	4	182	32	22	214	799	108	1	48	0
7	-356.25	208.75	73.75	0	3	8	191	24	22	241	705	107	1	51	1
8	-301.25	205	73.75	0	1	0	268	43	31	295	301	48	1	36	0
9	-241.25	205	73.75	0	1	0	397	38	47	299	40	37	1	12	0
10	-353.75	27.5	0	2	334	1587	398	182	134	2	3	6	0	2	2
11	-403.75	96.25	0	0	10	6	234	26	2172	30	75	3080	0	23	38
12	-377.5	193.75	5	0	30	0	268	132	37	165	80	11971	130	89	677
13	-321.25	223.75	0	0	1	0	287	28	34	350	72	3115	261	158	341
14	-275	241.25	0	0	1	1	495	41	60	386	50	877	318	50	83
15	-220	182.5	0	5	37	31	531	191	64	99	58	23	1	3	0
16	-320	167.5	5	6	153	411	339	585	44	47	95	9	0	4	0
17	-413.75	152.5	10	0	8	2	254	51	166	135	63	10916	1	15	231
18	-413.75	176.25	10	0	5	1	260	45	121	145	64	12399	45	32	594
19	-413.75	200	10	0	6	0	263	49	52	185	69	12616	83	45	1120
20	-413.75	223.75	10	0	2	2	284	44	38	241	75	9059	92	50	1513
21	-413.75	247.5	10	0	1	1	299	52	35	295	77	5892	98	61	2330
22	-390	247.5	10	0	0	1	321	34	37	328	71	4040	218	63	1401
23	-367.5	247.5	10	0	0	1	327	34	38	348	67	3514	266	59	868
24	-343.75	247.5	10	0	0	1	338	30	40	351	64	3234	294	52	547
25	-311.25	247.5	10	0	0	2	392	31	46	359	57	2537	320	60	251
26	-282.5	148.75	0	8	108	445	317	436	43	38	75	18	1	3	2
27	-306.25	113.75	0	7	170	660	352	449	51	27	22	9	0	2	2
28	-270	102.5	0	10	154	705	402	303	57	24	16	8	1	2	1
29	0	0	0	0	1	4	1	2	0	0	0	1	0	0	0
30	-292.5	65	0	7	260	1226	382	238	64	11	8	9	1	2	3
31	-2.5	235	12.5	3	2	6	1	2	0	1	1	2	1	1	0
32	-2.5	275	12.5	2	2	3	0	1	0	1	1	1	3	1	0
33	-2.5	315	12.5	1	1	2	0	1	0	0	1	1	2	1	0

Table 9 Concentration Results II (BRC)

1. Bridge exhaust = 76.27 cu m/s
2. BRC roof exhaust = 37.76 cu m/s
3. Traffic exhaust = 4.5 cu m/s

Wind speed = 4.4 m/s at 10 m for Run No.1 - 8.
Wind speed = 8.8 m/s at 10 m for Run No.9 - 16.

K = Conc * U / Q U: Wind Speed Q: Exhaust flow rate

Point No.	X (ft)	Y (ft)	Z (ft)	Run No. 5 S1	Run No. 5 K S2	Run No. 5 S3	Run No. 6 S1	Run No. 6 K S2	Run No. 6 S3	Run No. 7 S1	Run No. 7 K S2	Run No. 7 S3	Run No. 8 S1	Run No. 8 K S2	Run No. 8 S3
1	-367.5	-45	73.75	0	37	0	0	26	1	0	103	79	0	386	1
2	-367.5	105	73.75	0	273	0	0	355	2	0	32	125	0	24	1
3	-350	162.5	73.75	0	320	0	0	67	3	0	50	187	0	13	1
4	-332.5	167.5	73.75	0	221	0	0	121	2	0	35	203	0	3	1
5	-213.75	180	73.75	1	381	0	0	95	2	0	30	154	0	3	1
6	-362.5	193.75	73.75	0	569	0	0	62	5	0	12	94	0	1	1
7	-356.25	208.75	73.75	0	586	0	0	39	6	0	7	89	0	1	1
8	-301.25	205	73.75	62	169	8	0	188	3	0	7	88	0	14	2
9	-241.25	205	73.75	26	13	2	0	637	3	0	417	96	0	5	1
10	-353.75	27.5	0	0	1	1	0	2	15	1	115	349	0	393	71
11	-403.75	96.25	0	0	40	8	0	1	38	0	1	280	0	2	8
12	-377.5	193.75	5	1	34	36	0	7	63	0	4	175	0	1	9
13	-321.25	223.75	0	247	70	46	0	363	80	0	5	231	0	1	4
14	-275	241.25	0	611	152	82	1	200	177	1	37	265	0	1	4
15	-220	182.5	0	2	3	0	0	27	10	0	26	496	0	119	19
16	-320	167.5	5	0	2	0	0	92	9	0	36	546	0	206	34
17	-413.75	152.5	10	0	22	32	0	1	80	0	1	319	0	1	11
18	-413.75	176.25	10	0	22	44	0	1	114	0	1	339	0	0	13
19	-413.75	200	10	1	23	57	0	1	156	0	1	387	0	0	15
20	-413.75	223.75	10	1	17	63	0	1	215	0	1	467	0	0	15
21	-413.75	247.5	10	3	26	88	0	1	140	0	1	396	0	0	13
22	-390	247.5	10	13	23	41	0	6	157	0	1	418	0	0	10
23	-367.5	247.5	10	184	45	49	0	63	125	1	2	381	0	1	8
24	-343.75	247.5	10	415	59	75	1	75	127	1	2	332	0	1	8
25	-311.25	247.5	10	459	83	73	1	206	163	1	7	259	0	1	6
26	-282.5	148.75	0	1	2	0	0	54	9	0	19	495	0	226	41
27	-306.25	113.75	0	0	1	0	0	85	9	0	24	532	0	273	55
28	-270	102.5	0	0	1	1	0	24	14	0	13	592	0	189	25
29	0	0	0	1	2	1	1	2	1	2	2	4	0	2	0
30	-292.5	65	0	0	1	2	0	11	18	0	24	520	0	287	65
31	-2.5	235	12.5	15	2	2	0	337	279	0	6	401	0	2	7
32	-2.5	275	12.5	128	10	15	0	332	234	0	5	403	0	1	7
33	-2.5	315	12.5	276	22	33	1	216	154	1	4	218	0	1	4

Table 10 Concentration Results III (BRC)

1. Bridge exhaust = 76.27 cu m/s
2. BRC roof exhaust = 37.76 cu m/s
3. Traffic exhaust = 4.5 cu m/s

Wind speed = 4.4 m/s at 10 m for Run No.1 - 8.
Wind speed = 8.8 m/s at 10 m for Run No.9 - 16.

K = Conc * U / Q U: Wind Speed Q: Exhaust flow rate

				Run No. 9			Run No. 10			Run No. 11			Run No. 12		
Point No.	X (ft)	Y (ft)	Z (ft)	S1	K S2	S3	S1	K S2	S3	S1	K S2	S3	S1	K S2	S3
1	-367.5	-45	73.75	0	5928	27	262	2013	31	3	209	0	0	46	0
2	-367.5	105	73.75	0	40	20	212	2113	23	27	228	2	0	263	0
3	-350	162.5	73.75	0	52	49	207	360	23	128	1700	22	0	21	0
4	-332.5	167.5	73.75	0	61	65	219	465	23	152	1965	22	0	48	0
5	-213.75	180	73.75	0	23	22	204	103	22	183	1989	31	0	51	0
6	-362.5	193.75	73.75	0	5	2	178	22	22	225	2008	106	0	68	0
7	-356.25	208.75	73.75	0	11	4	186	20	22	244	1949	115	1	136	0
8	-301.25	205	73.75	0	3	0	250	26	27	288	1798	47	0	818	0
9	-241.25	205	73.75	0	1	0	378	30	45	331	48	39	1	7	0
10	-353.75	27.5	0	2	837	1078	408	494	131	2	8	4	0	2	0
11	-403.75	96.25	0	0	24	4	238	28	1408	45	217	4228	0	66	43
12	-377.5	193.75	5	0	27	6	274	83	43	203	124	12551	165	268	575
13	-321.25	223.75	0	0	1	4	286	28	35	396	114	3188	282	98	250
14	-275	241.25	0	0	1	0	465	38	57	437	66	645	327	51	66
15	-220	182.5	0	6	47	20	542	432	63	101	89	47	1	3	0
16	-320	167.5	5	2	225	147	325	2195	39	46	345	8	0	9	0
17	-413.75	152.5	10	0	7	8	257	47	139	162	122	11804	3	117	235
18	-413.75	176.25	10	0	3	8	259	31	106	172	114	13648	51	160	508
19	-413.75	200	10	0	4	10	262	30	51	207	118	13484	98	203	806
20	-413.75	223.75	10	0	2	8	281	31	47	275	118	9647	109	218	1079
21	-413.75	247.5	10	0	1	8	290	36	37	349	109	5393	121	251	1471
22	-390	247.5	10	0	1	6	315	30	37	383	96	3745	248	167	956
23	-367.5	247.5	10	0	1	4	324	30	39	398	85	3426	301	124	604
24	-343.75	247.5	10	0	1	2	333	29	41	407	77	2998	326	87	354
25	-311.25	247.5	10	0	1	4	384	31	45	414	76	2403	341	61	190
26	-282.5	148.75	0	7	323	375	311	1584	41	37	233	12	1	7	0
27	-306.25	113.75	0	7	497	491	349	1574	47	27	75	6	1	5	0
28	-270	102.5	0	10	330	440	403	1118	55	22	55	8	1	4	0
29	0	0	0	0	2	2	1	6	0	1	2	0	1	1	0
30	-292.5	65	0	8	585	833	390	683	61	10	21	6	0	4	4
31	-2.5	235	12.5	3	3	4	2	4	0	1	1	0	0	0	0
32	-2.5	275	12.5	2	1	2	1	1	2	0	1	2	3	1	2
33	-2.5	315	12.5	0	1	4	0	1	0	0	1	2	2	1	2

Table 11 Concentration Results IV (BRC)

1. Bridge exhaust = 76.27 cu m/s
2. BRC roof exhaust = 37.76 cu m/s
3. Traffic exhaust = 4.5 cu m/s

Wind speed = 4.4 m/s at 10 m for Run No.1 - 8.
Wind speed = 8.8 m/s at 10 m for Run No.9 - 16.

K = Conc * U / Q U: Wind Speed Q: Exhaust flow rate

				Run No. 13			Run No. 14			Run No. 15			Run No. 16		
Point No.	X (ft)	Y (ft)	Z (ft)	S1	K S2	S3	S1	K S2	S3	S1	K S2	S3	S1	K S2	S3
1	-367.5	-45	73.75	0	57	0	0	24	0	1	124	72	0	665	0
2	-367.5	105	73.75	0	3696	0	0	536	0	1	14	94	0	13	0
3	-350	162.5	73.75	0	1544	0	0	215	0	1	36	154	0	10	0
4	-332.5	167.5	73.75	0	1093	0	0	692	0	1	43	166	0	4	0
5	-213.75	180	73.75	1	1296	0	0	377	0	0	30	121	0	4	0
6	-362.5	193.75	73.75	0	1838	0	0	142	0	0	10	65	0	2	0
7	-356.25	208.75	73.75	0	1662	0	0	125	0	1	8	63	0	2	0
8	-301.25	205	73.75	38	734	2	0	1031	0	1	16	68	0	41	0
9	-241.25	205	73.75	29	37	2	0	2245	0	0	2913	76	0	47	0
10	-353.75	27.5	0	0	2	0	0	10	2	1	94	297	0	735	41
11	-403.75	96.25	0	0	69	10	0	2	6	0	2	213	0	3	6
12	-377.5	193.75	5	0	103	33	0	5	18	1	2	125	0	1	8
13	-321.25	223.75	0	212	135	37	0	371	25	1	6	170	0	2	0
14	-275	241.25	0	595	137	76	1	488	96	1	29	207	0	2	0
15	-220	182.5	0	1	3	0	0	176	0	1	123	456	0	223	10
16	-320	167.5	5	0	4	0	0	596	0	1	121	473	0	339	20
17	-413.75	152.5	10	0	52	35	0	3	20	1	2	213	0	1	10
18	-413.75	176.25	10	0	44	45	0	1	27	1	1	235	0	0	12
19	-413.75	200	10	0	43	55	0	1	35	1	1	282	0	0	14
20	-413.75	223.75	10	1	37	49	0	2	70	1	1	330	0	0	12
21	-413.75	247.5		3	59	49	0	24	23	1	2	227	0	0	4
		247.5		12	73	29	0	47	29	1	2	299	0	0	6
				57	115	39	0	120	35	1	3	270	0	1	4
				57	110	61	1	153	53	1	3	241	0	1	2
25		247.5		391	128	61	1	301	78	1	6	194	0	1	2
26	-282.5	148.75	0	1	4	0	0	393	0	1	91	454	0	407	25
27	-306.25	113.75	0	0	3	0	0	566	0	1	135	462	0	519	35
28	-270	102.5	0	0	2	0	0	179	0	1	70	532	0	338	14
29	0	0	0	0	1	0	0	2	0	2	2	0	0	2	0
30	-292.5	65	0	0	3	2	0	72	2	0	118	436	0	571	41
31	-2.5	235	12.5	16	2	2	0	793	186	0	12	383	0	3	4
32		235		19	11	18	0	734	153	1	10	385	0	2	2
				35	26	39	1	454	96	1	7	211	0	1	2

FIGURES

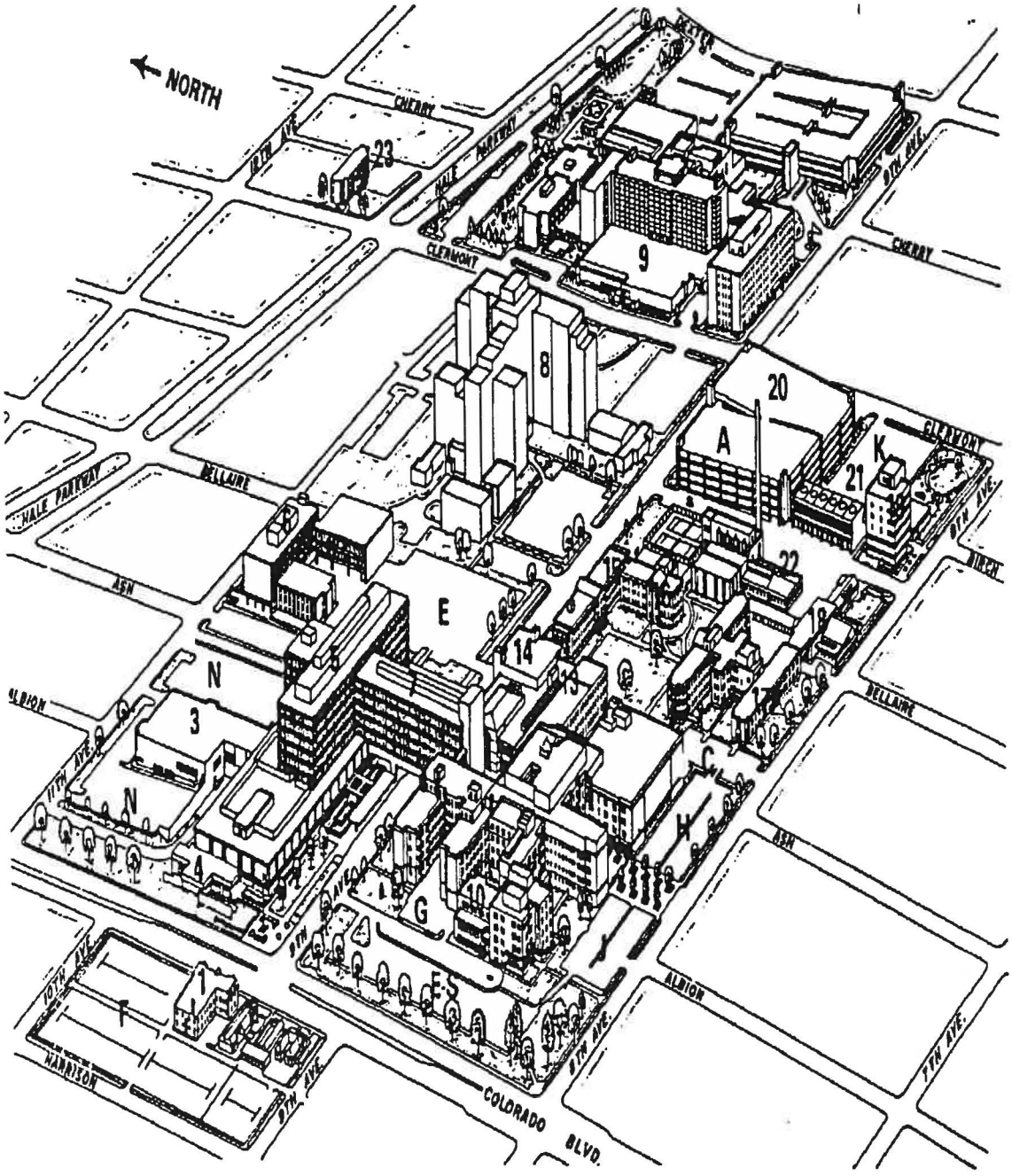

Figure 1 Top View of the University of Colorado Health Sciences Center and Surrounding Buildings

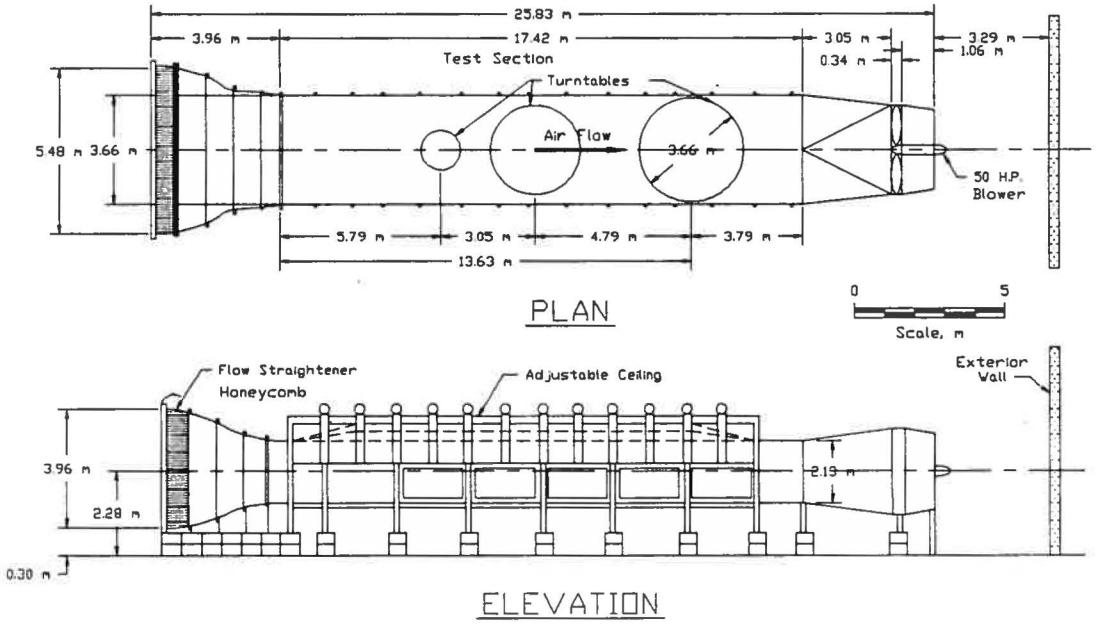

Figure 2 Environmental Wind Tunnel

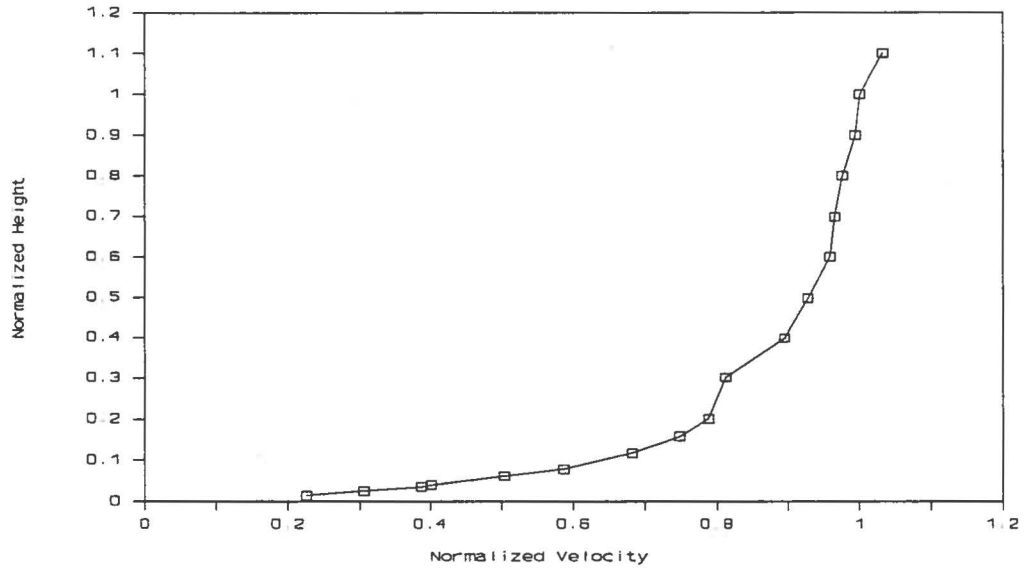

Figure 3 Velocity Profile

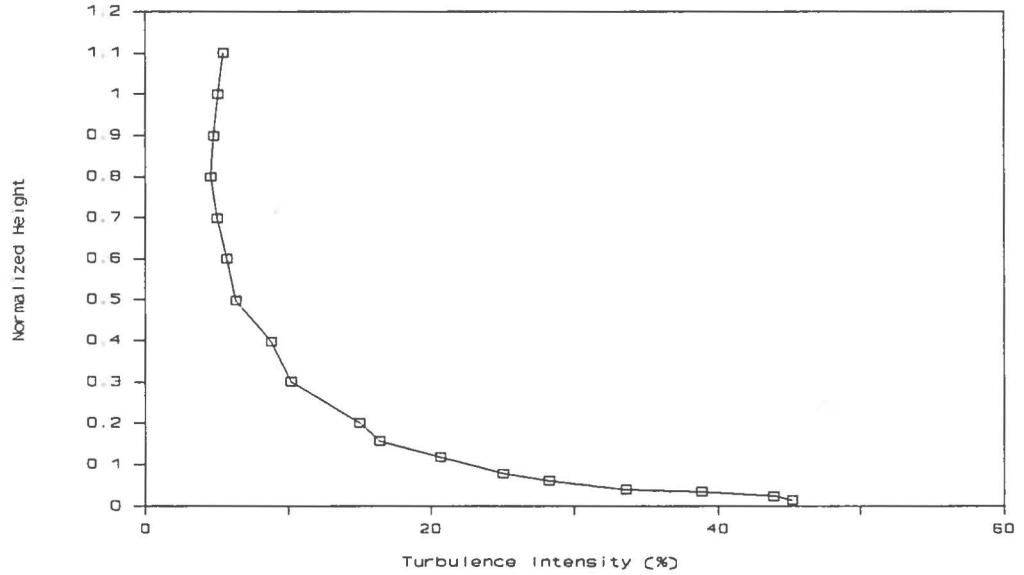

Figure 4 Turbulence Profile

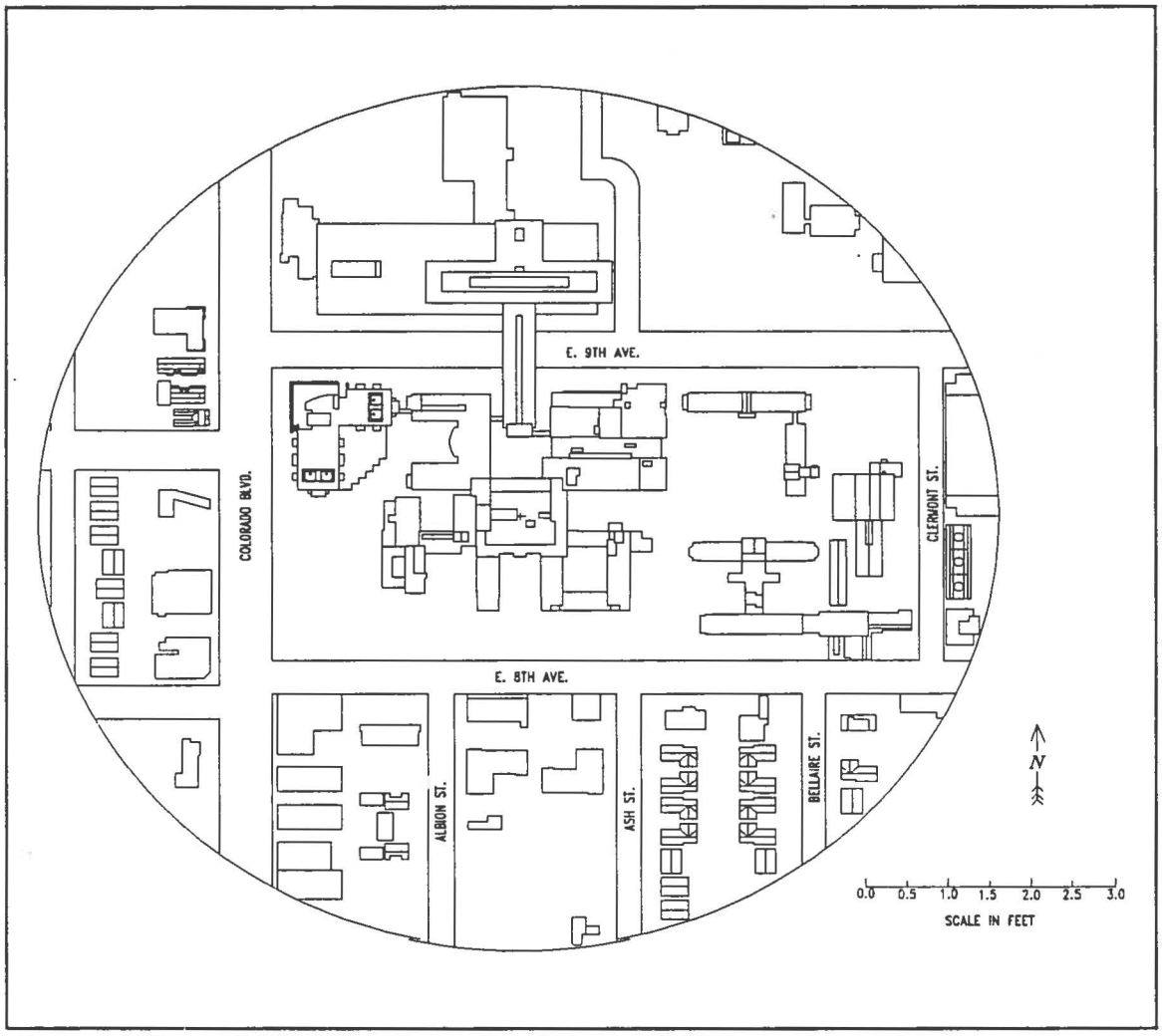

Figure 5 Map of UCHSC and surrounding buildings

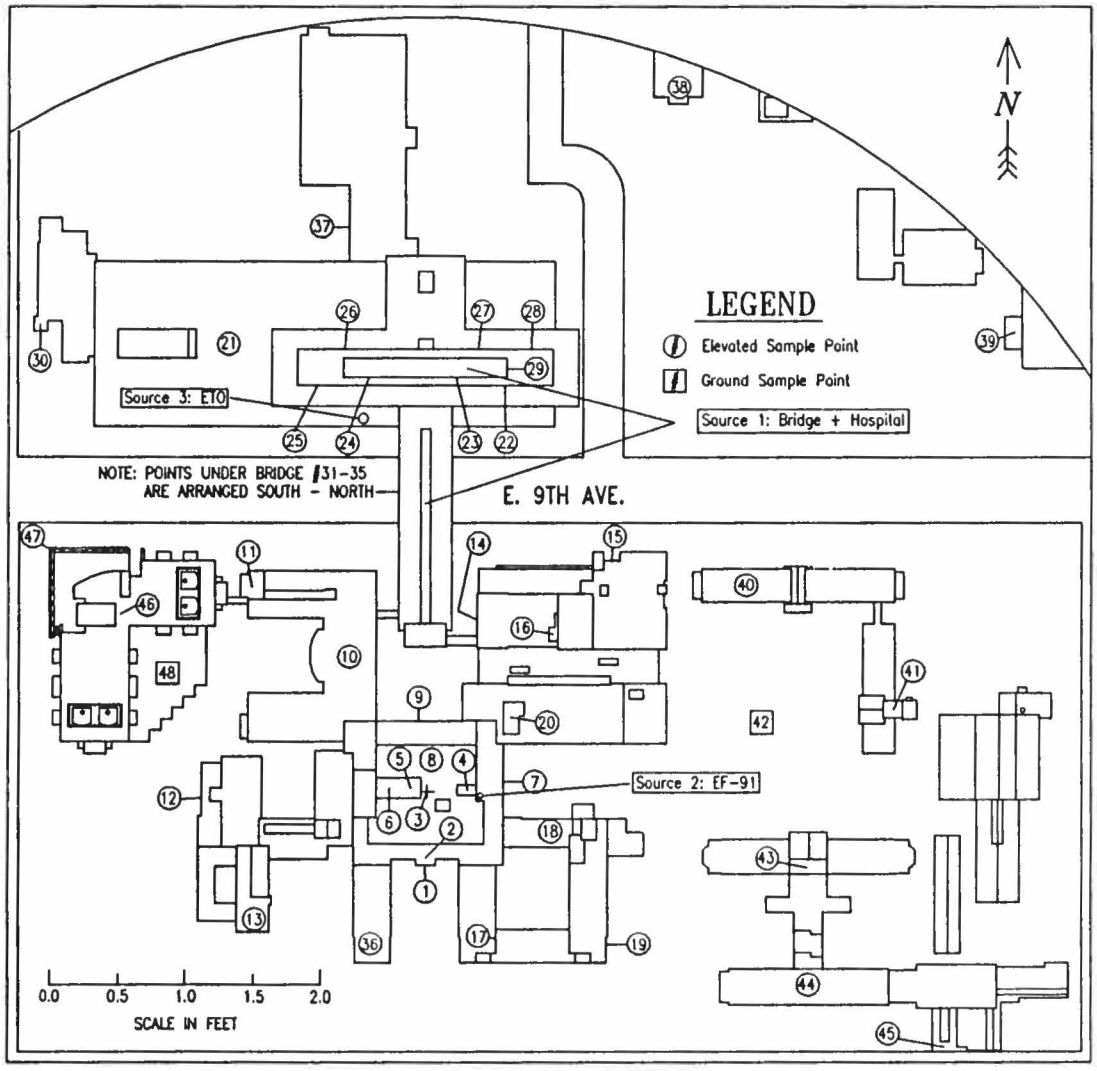

Figure 6 Sampling Point Diagram for the School of Medicine

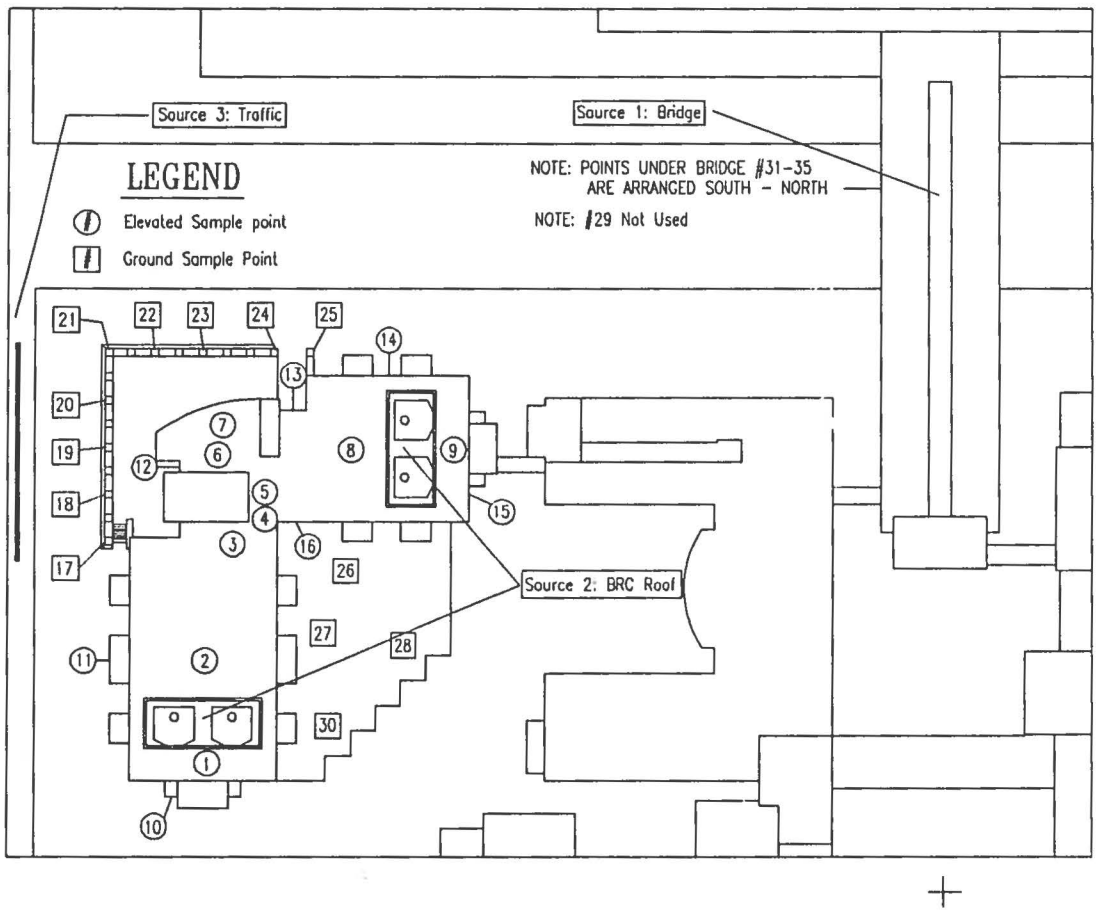

Figure 7 Sampling Point Diagram for the Biomedical Research Center

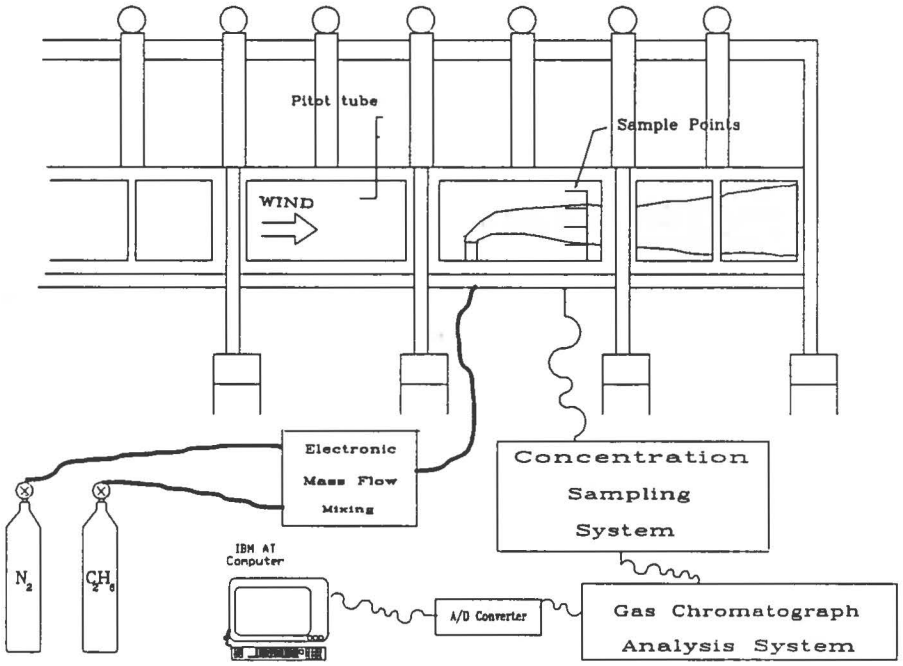

Figure 8 Wind Tunnel Gas Release and Sampling Schematic

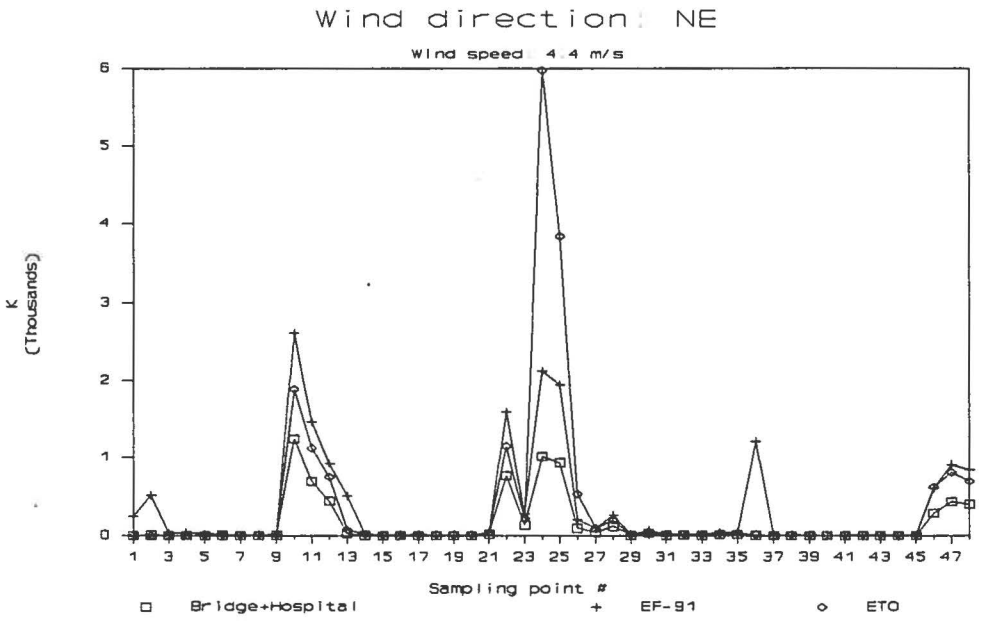

Figure 9 Concentration Level at NE Wind Direction for Low Speed Conditions

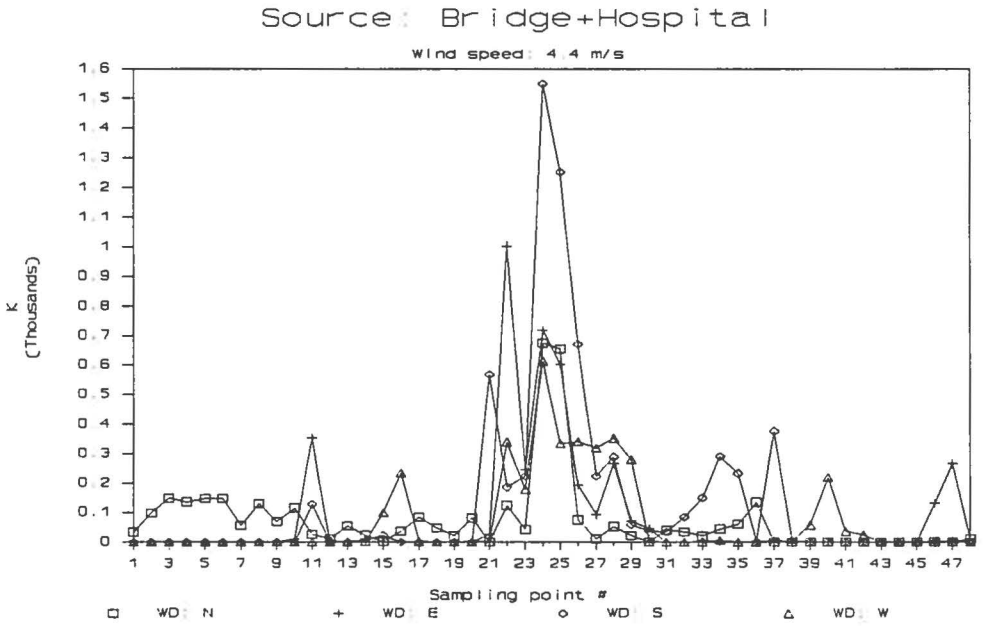

Figure 10 Concentration Level for Four Wind Directions for Bridge & Hospital Exhausts

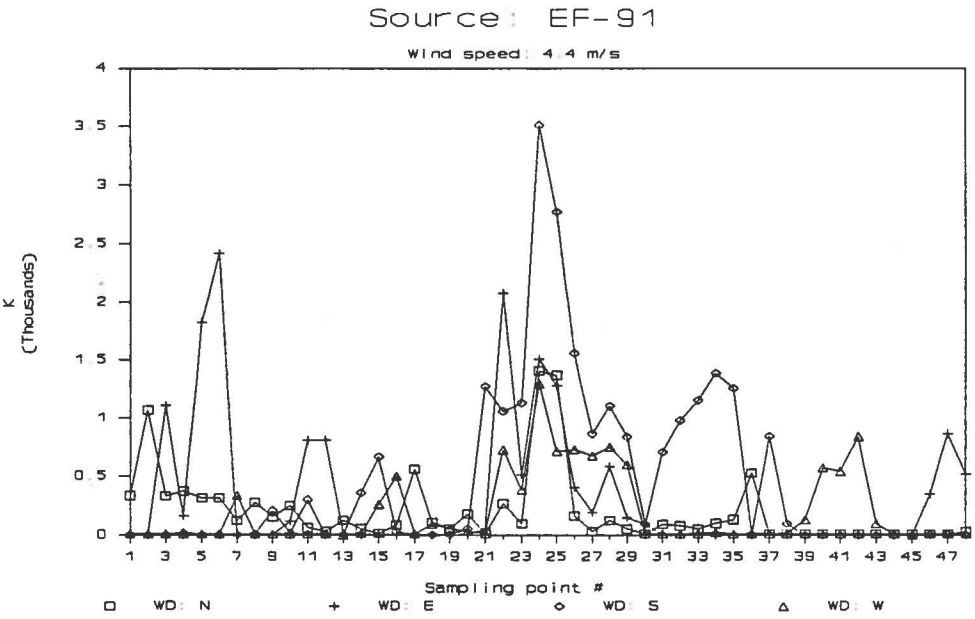

Figure 11 Concentration Level for Four Wind Directions for Source EF-91

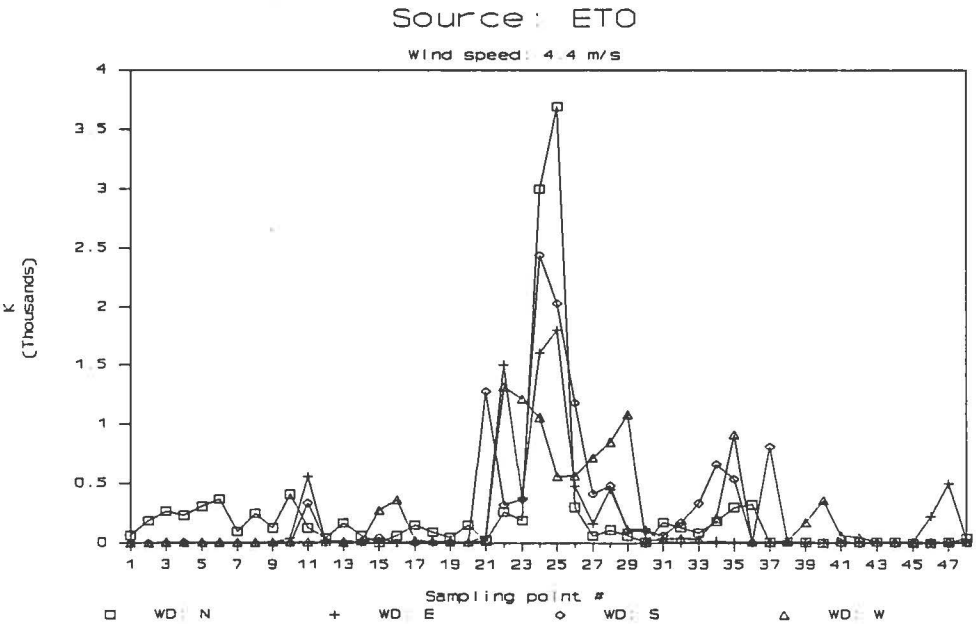

Figure 12 Concentration Level for Four Wind Directions for Source ETO

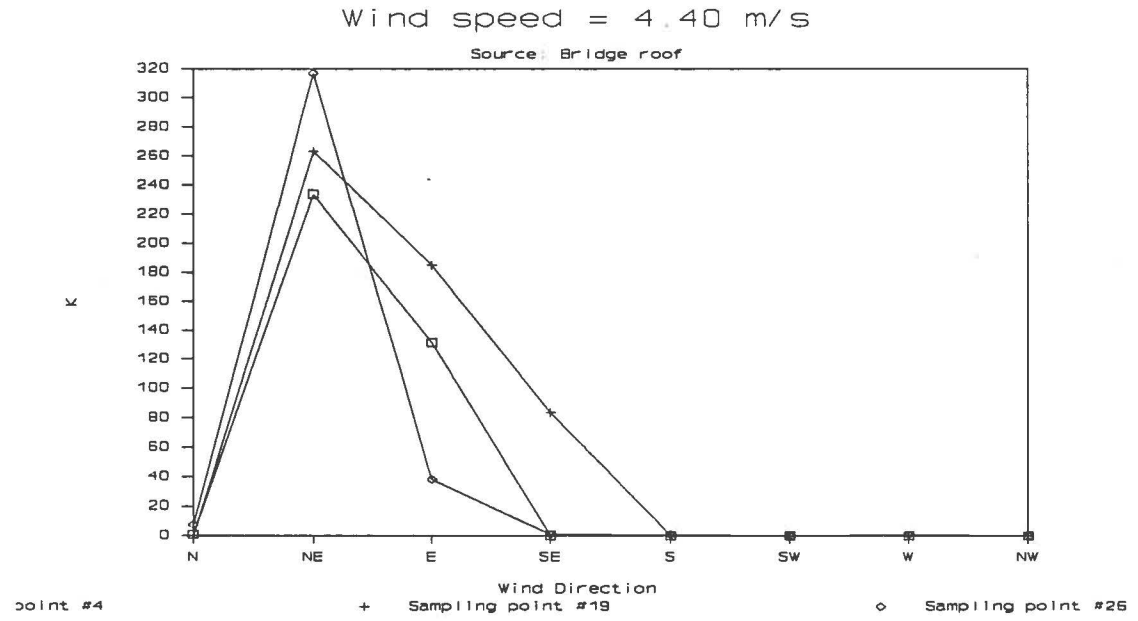

Figure 13 Concentration Level at Locations #4,19 and 26 for Bridge Exhaust

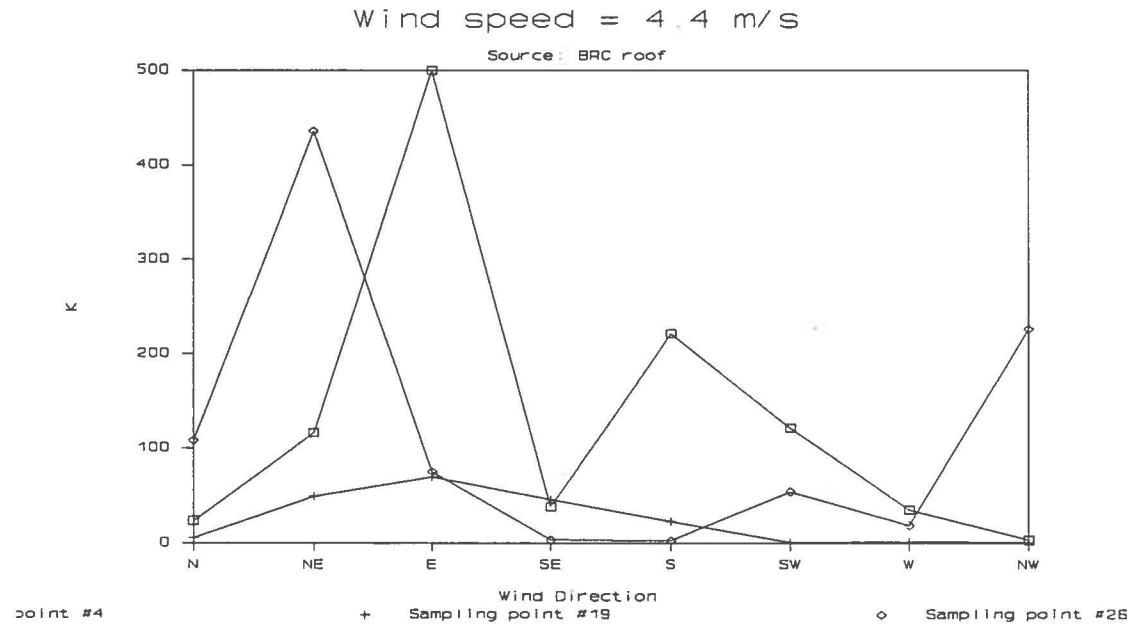

Figure 14 Concentration Level at Locations #4,19 and 26 for BRC Roof Exhaust

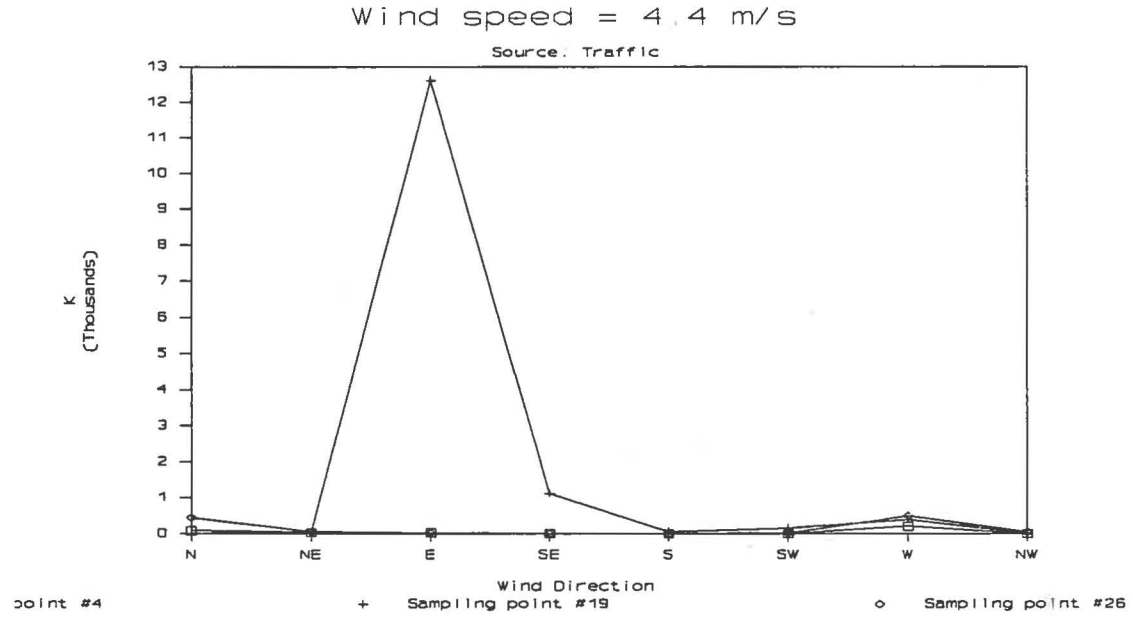

Figure 15 Concentration Level at Locations #4,19 and 26 for Traffic Exhaust

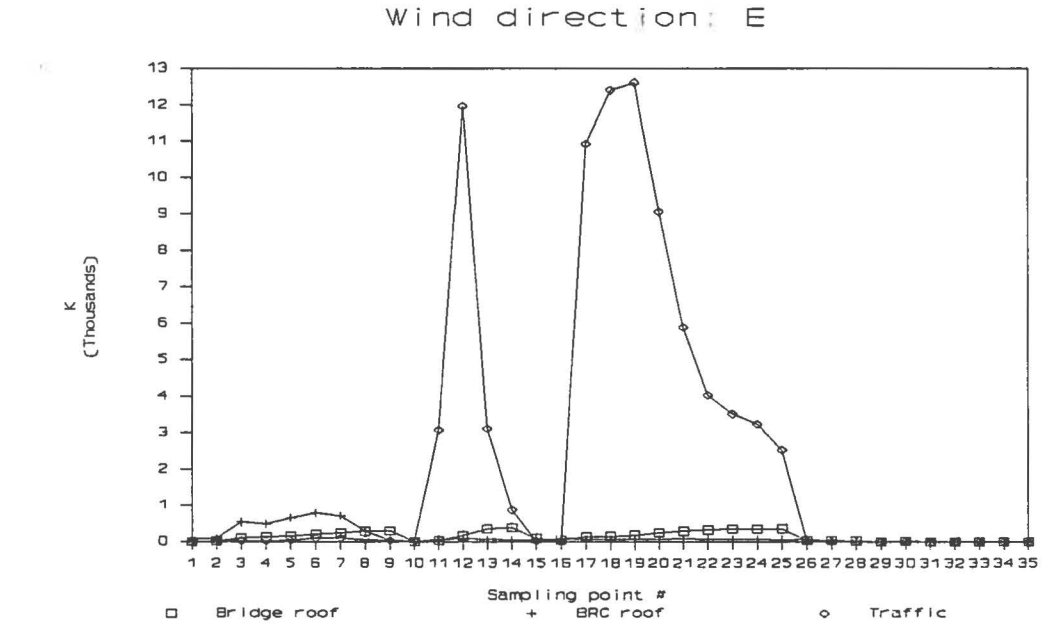

Figure 16 Concentration Level for East Wind Direction and Low Speed Conditions

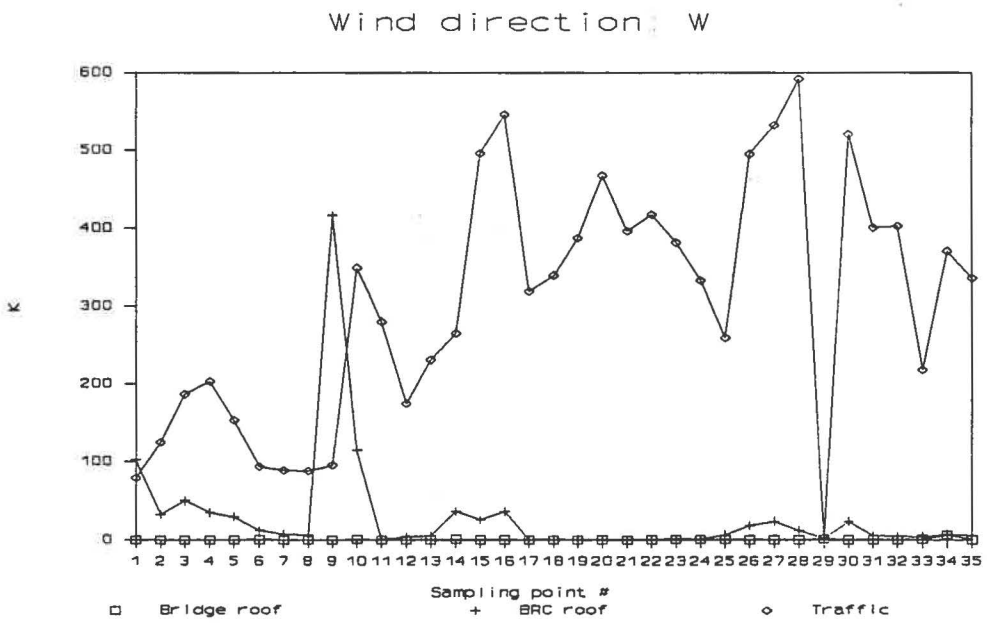

Figure 17 Concentration Level for West Wind Direction and Low Speed Conditions

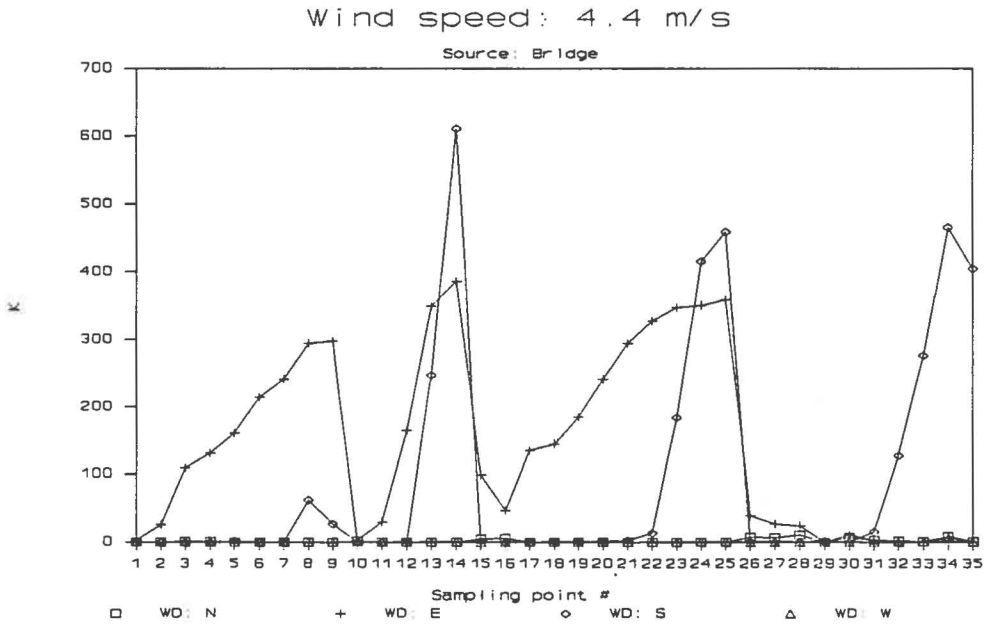

Figure 18 Concentration Level for Four Wind Directions and Bridge Exhaust

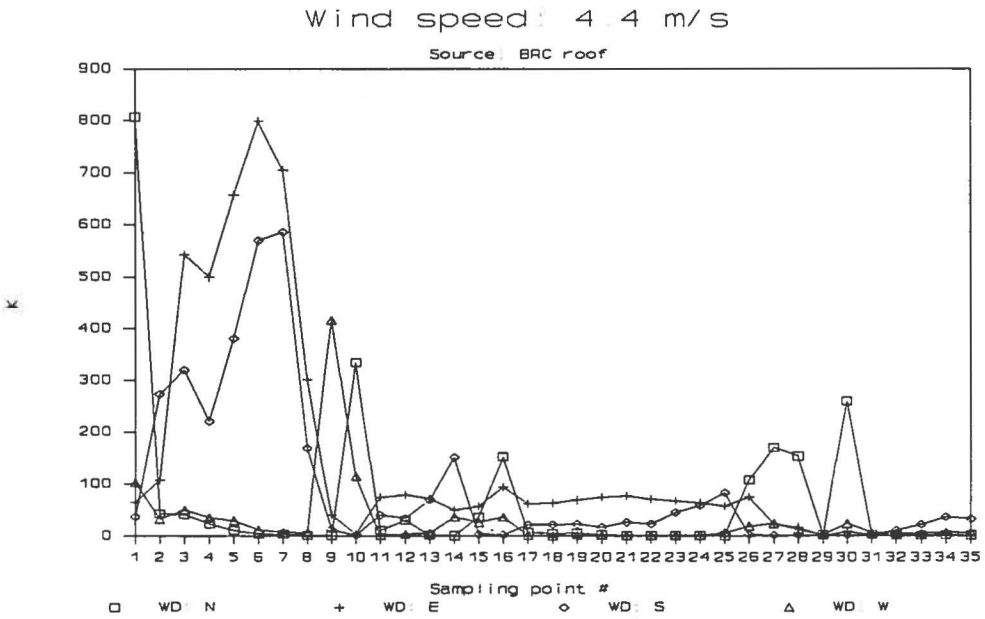

Figure 19 Concentration Level for Four Wind Directions and BRC Exhaust

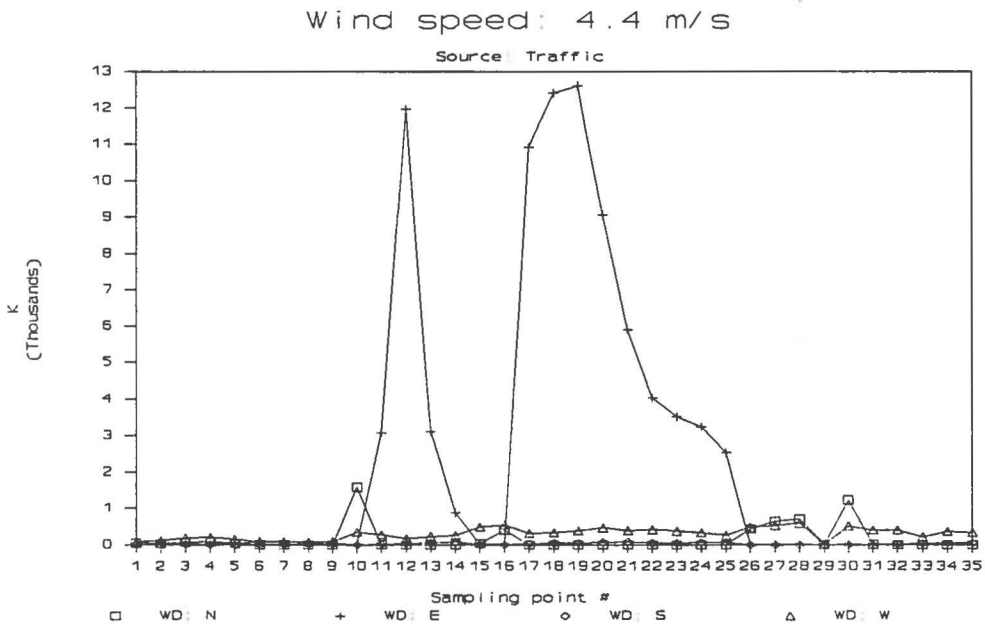

Figure 20 Concentration Level for Four Wind Directions and Traffic Exhaust

APPENDIX: MODELING OF PLUME DISPERSION

To obtain a predictive model for a specific plume dispersion problem, one must quantify the pertinent physical variables and parameters into a logical expression that determines their inter-relationships. This task is achieved implicitly for processes occurring in the atmospheric boundary layer by the formulation of the equations of conservation of mass, momentum and energy. These equations with site and source conditions and associated constitutive relations are highly descriptive of the actual physical interrelationship of the various independent variables (space and time) and dependent variables (velocity, temperature, pressure, density, concentration, etc.).

These generalized conservation statements subject to the typical boundary conditions of atmospheric flow are too complex to be solved by present analytical or numerical techniques. It is also unlikely that one could create a physical model for which exact similarity exists for all the dependent variables over all the scales of motion present in the atmosphere. Thus, one must resort to various degrees of approximation to obtain a predictive model. At present, purely analytical or numerical solutions of boundary layer, wake, and plume dispersion are unavailable because of the classical problem of turbulent closure (Hinze, 1975). However, boundary layer wind tunnels are capable of physically modeling plume processes in the atmosphere under certain restrictions. These restrictions are discussed in the next sections.

A.1 FLUID MODELING OF THE ATMOSPHERIC BOUNDARY LAYER

The atmospheric boundary layer is that portion of the atmosphere extending from ground level to a height of approximately 1000 meters within which the major exchanges of mass, momentum, and heat occur. This region of the atmosphere is described mathematically by statements of conservation of mass, momentum and energy (Cermak, 1975). The mathematical requirements for rigid laboratory/atmospheric-flow similarity may be obtained by fractional analysis of these governing equations (Kline, 1965). This methodology scales the pertinent dependent and independent variables by size and then casts the equations into dimensionless form by dividing by one of the coefficients (the inertial terms in this case). Performing these operations on such dimensional equations yields dimensionless parameters commonly known as:

Reynolds number	$Re = (UL/\nu)_r$	=	$\frac{\text{Inertial Force}}{\text{Viscous Force}}$
Bulk Richardson number	$Ri = [(Lg\Delta T/T)/U^2]_r$	=	$\frac{\text{Gravitational Force}}{\text{Inertial Force}}$
Rossby number	$Ro = (U/L\Omega)_r$	=	$\frac{\text{Inertial Force}}{\text{Coriolis Force}}$

Prandtl number $Pr = [\nu/(k/\rho C_p)]_r = \frac{\text{Viscous Diffusivity}}{\text{Thermal Diffusivity}}$

Eckert number $Ec = [U^2/C_p\Delta T]_r$

A.1.1 Exact Similarity

For exact similarity between flows which are described by the same set of equations, each of these dimensionless parameters must be equal for both flow systems. There must also be similarity between the surface-boundary conditions and the approach flow wind field. Surface-boundary condition similarity requires equivalence of the following features:

a. Surface-roughness distributions,
b. Topographic relief, and
c. Surface-temperature distribution.

If all the foregoing requirements are met simultaneously, all atmospheric scales of motion ranging from micro- to mesoscale could be simulated within the same flow field. However, all of the requirements cannot be satisfied simultaneously by existing laboratory facilities; thus, a partial or approximate simulation must be used. This limitation requires that atmospheric simulation for plume dispersion must be designed to simulate most accurately those scales of motion which are of greatest significance for the transport and dispersion of plumes.

A.1.2 Partial Simulation of the Atmospheric Boundary Layer

For many fluid modeling situations several of the aforementioned parameters are unnecessarily restrictive and may be relaxed without causing a significant loss in similarity between model and field fluid flow. The Rossby number magnitude controls the extent to which the mean wind direction changes with height. The effect of Coriolis-force-driven lateral wind shear on wind flow is only significant when heights are of the same order of magnitude as the boundary layer height. The Eckert number (in air $Ec = 0.4\ Ma^2\ (T_r/\Delta T_r)$, where Ma is the Mach number) is the ratio of energy dissipation to the convection of thermal energy. Both in the atmosphere and the laboratory flow, the wind velocities and temperature differences are such that the Eckert number is very small; hence, it is neglected. Prandtl number equality guarantees equivalent rates of momentum and heat transport. Since air is the working fluid in both the atmosphere and the laboratory, Prandtl number equality is always maintained.

The approach flow Richardson number (Ri) and Reynolds number (Re) determine the kinematic and dynamic structure of turbulent flow within a boundary layer. This influence is apparent in the variations that occur in the spectral distribution of turbulent kinetic energies with changing Ri and changing Re.

The Reynolds Number

Re equality implies $U_m = (L_p/L_m)U_p$. Re equality at a significantly reduced length scale would cause the model's flow velocity to be above sonic; hence, its equality must be distorted. A reduced Re changes only the higher frequency portion of an Eulerian-type description of the spectral energy distribution. Unfortunately, there is no precise definition as to which portion of an Eulerian Spectrum is dominant in dispersing ground-level or elevated plumes over moderate travel distances.

Most investigators use a minimum Reynolds number requirement based on rough-walled pipe measurements; i.e., $Re = u_* z_o/\nu > 2.5$, where u_*, the friction velocity, and z_o, the roughness length, are derived from a log-linear fit to a measured mean velocity profile. The value 2.5 is an empirically determined constant. At Re below 2.5, it is observed that the mean velocity profiles in turbulent pipe flow lose similarity in shape and deviate from the universal curve of a rough wall turbulent boundary layer. For Re above 2.5, it is observed that the surface drag coefficient (and thus the normalized mean velocity profile) is invariant with respect to increasing Re. For Re between 0.11 and 2.5, the velocity profiles are characteristic of smooth wall turbulent boundary layers. For values below 0.11, the growth of a laminar sublayer on the wall is observed to increase with decreasing Re.

Extrapolation of results from pipe flow measurement to flat plate boundary layers may cause a shift in the magnitude of the minimum Re requirement, but it is generally felt that this shift is small. Precise similarity in the universal form of mean wind shear may be necessary for invariance with respect to the surface drag coefficient, but this does not necessitate that precise similarity must exist for the invariance of the wind field and dispersion. It is the distribution of turbulent velocities which has the greatest effect on the wind field and dispersion. It is the mean wind shear, however, which generates the turbulent velocities. It is possible that the specification of a minimum Re of 2.5 is overly conservative. The criteria, Re > 2.5, for example, is not applicable for flow over complex terrain or building clusters.

The Richardson Number

Although most wind-tunnel investigations are conducted with neutrally stratified boundary layers, there are circumstances when the stratification of the atmosphere must be considered. In particular, air pollution and dispersion problems are often critical during stratified conditions. Unstable stratification may be expected to mitigate hazards by accelerating plume dilution, whereas stable stratification may permit high concentrations to persist. The stability state of the atmosphere is typically characterized by the Richardson number.

The atmospheric gradient Richardson number can be computed from averaged quantities through the equation

$$Ri = g/T\ (\Gamma_d - \Gamma)\ [1 + 0.07/B]\ [(\partial u/\partial z)^2 + (\partial v/\partial z)^2]$$

where Γ and Γ_d are the actual and dry adiabatic potential temperature lapse rates, and $B = [C_p(T_2-T_1)]/[(Z_2-Z_1)(Q_2-Q_1)]$ is the Bowen ratio of sensible to latent heat flux at the surface. The Ri number can be taken to represent the ratio of the relative importance of convective and mechanical turbulence. Negative Ri numbers of large value indicate strong convection and weak mechanical turbulence; zero Ri numbers imply purely mechanical turbulence. Positive Ri numbers less than some critical value, $Ri_{critical}$, suggest the presence of mechanical turbulence damped by the density-induced buoyancy forces; for larger positive Ri numbers, turbulence essentially disappears, since the stratification overpowers production by wind shear. The critical Richardson number has a value near 0.25.

A.1.3 Performance of Prior Fluid Modeling Experiments

Meroney et al. (1978) summarized experimental data available from field and laboratory studies for neutral airflow over hills, ridges, and escarpments. Wind-tunnel model measurements were performed to study the influence of topography profile, surface roughness and stratification on the suitability of various combinations of these variables. Detailed tables of velocity, turbulence intensity, pressure, spectra, etc., were prepared to guide numerical model design and experimental rule of thumb restrictions. Cases included hill slopes from 1:2 to 1:20, neutral and stratified flows, two- and three-dimensional symmetric ridges, six alternate hill and escarpment shapes, and a variety of windward versus leeward slope combinations to evaluate ridge separation characteristics. The laboratory data were validated by comparison with field measurements for flow in the Rakaia Gorge, New Zealand, and over Kahuku Point, Oahu, Hawaii, (Meroney et al., 1978; Chien, Meroney and Sandborn, 1979).

Local heating and cooling of coastline or hill surfaces are the driving mechanisms for sea-land breezes, and anabatic and katabatic winds which may inhibit or enhance airflow over the land surface. Early laboratory work includes simulations of urban heat islands by Yamada and Meroney (1971) and Sethuraman and Cermak (1973), simulation of flow and dispersion at shoreline sites by Meroney et al. (1975a), and simulation of dispersion effects of heat rejected from large industrial complexes by Meroney et al. (1975b).

Meroney (1980) compared three model/field investigations of flow over complex terrain, suggested performance envelopes for realizable modeling in complex terrain, and discussed recent laboratory studies which provide data for valley drainage flow situations. Not all of the model/field comparison experiments performed in the past were successful. Many early studies had model approach flow velocity exponents near zero, were modeled as neutral flows when the field observed strong stratification effects, or simulated unrealistic boundary layer depths, integral scales, or turbulence intensities which did not match their atmospheric counterpart. But few studies claimed unreasonable correlation, and some were strongly self-critical. Nonetheless, most studies accomplished their prestated limited objectives. It would appear

that the simulation hypothesis developed in the last few years is appropriate for physical modeling of flow over complex terrain when appropriate care is taken to simulate the approach flow conditions and to maintain simulation parameters equal between model and prototype.

Arya and Plate (1969), Arya (1975) performed velocity, temperature, and turbulence measurements in the lowest 15 percent of a 70 cm deep boundary layer over a smooth surface, where conditions ranged from unstable to moderately stable ($-0.3 < z/L_{mo} < 0.3$). Free stream flow speeds varied from 3 to 9 m/s, and temperature differences were about 40°C across the boundary layer. Cermak, Shrivastava and Poreh (1983) reported mean velocity and turbulence measurements made for a variety of simulated atmospheric boundary layers over different surface roughness. Free stream flow speeds varied from 2.4 to 3.0 m/s and temperature differences were from 150°C to -80°C across the boundary layer. Poreh and Cermak (1984) reproduced unstable lapse conditions including mixed layers and elevated inversions. They reproduced the characteristics of convective boundary layer turbulence measured in the atmosphere.

Diffusion studies made by Chaudhry and Meroney (1973) in stable boundary layers investigated previously by Arya (1969) have shown agreement of experimental results with Lagrangian similarity theory. Horst (1979) tested Lagrangian similarity predictions of crosswind-integrated ground concentration against the Prairie Grass diffusion experiment (Barad, 1958) and an experiment at Idaho Falls (Islitzer and Dumbauld, 1963). He reported good agreement for all stabilities at distances x/z_o out to $2*10^5$. Poreh and Cermak (1984, 1985) released plumes in their modeled mixing layer. Their plumes exhibited the plume lofting typical of ground sources and the descent typical of elevated sources, predicted from water tank experiments by Willis and Deardorff (1974, 1976, 1978) and numerically by Lamb (1982).

Staff at the Fluid Mechanics Laboratory at the Ecole Centrale de Lyon have studied unstable wind-tunnel boundary layers and compared them with the atmospheric boundary layer (Schon and Mery, 1971). Flow speeds were typically 2 to 4 m/s and the floor temperature was maintained 50°C above ambient. Comparisons with the Kansas data (Haugen et al., 1971) were quite satisfactory, but longitudinal turbulence intensities exhibited a slight Reynolds number dependence, and spectral energy was too low in the high frequency portions of the spectra. The most unstable flow they studied had a Monin-Obukhov scale length of about -1 m at model scales, or -500 to -1000 when scaled to the atmosphere.

A.2 PHYSICAL MODELING OF BLUFF BODY AERODYNAMICS

The interaction of an approach wind field with bluff bodies or structures constructed on the earth's surface is broadly termed "Building Aerodynamics." In a review article on this subject, Meroney (1982) discusses the character of bluff body flow about rectangular buildings and cylindrical cooling towers. Defects in velocity profiles can easily persist from 10 to 15 building heights downwind. Field and laboratory measurements of plume dispersion about the Rancho Seco Nuclear Power

Station in Sacramento, California, confirm that cooling tower wake effects persist for significant downwind distances under a variety of stratification conditions (Allwine, Meroney and Peterka, 1978; Kothari, Meroney and Bouwmeester, 1981).

A.2.1 Simulation Criteria

Often atmospheric turbulence may cause only weak effects compared to the turbulence generated by buildings, obstacles, and terrain. Yet the magnitude of the perturbations depends upon the incident flow turbulence scale and intensity, details of the obstacle shape and surface roughness, and size of the obstacle compared to the boundary layer depth. Geometrical scaling implies that the ratio of the building height to length scale must be matched and, of course, that all other building length scales be reduced to this same ratio.

Several questions should be considered when modeling flows which include surface obstacles:

a. What size obstacles should be disregarded?
b. What detail or roughness on an obstacle need be included?
c. To what upwind distance should all obstacles be included?
d. At what point does the size of a modeled obstacle become too big for the wind tunnel (i.e., blockage effects)?
e. What is the effect on the flow field of mismatching obstacle and approach flow length scales?
f. What is the minimum allowable model obstruction Reynolds number?

Obstacle sizes to be disregarded:

Boundary layer studies of rough surfaces reveal that if protuberances are of a size k, such that $u_*k/\nu < 5$, they will have little effect on the flow in a turbulent boundary layer. Thus, assuming a laboratory wind speed of 1 m/s and a typical friction coefficient $C_f/2 = (u_*/u)^2 = 0.0025$, obstacles of size less than 2 mm would go unnoticed.

Required obstacle surface detail or roughness:

Another question that always arises is "How much detail is required for the building or obstacle model? The answer is, of course, dependent upon the size of the protuberance compared to the plume and the dominant eddies of mixing. If the obstruction is large enough to modify the separated wake over the main obstacle, then it must be included. Often an equivalent obstacle surface roughness suffices. Snyder (1981) concludes a generic surface roughness criterion might be $u_*k/\nu > 20$. For a 1 m/s laboratory flow this results in model roughness elements equal to about 6 mm. But since the exterior flow is usually highly turbulent, the body typically includes a highly unsteady wake, and the u_* value to be used should be that acting on the building surface, rather than that of the approach flow. Hence, even this roughness may be unnecessarily large.

Upstream fetch to be modeled:

Suppose there is another building, tree line, fence, cooling tower, or obstacle some distance, s, upstream of a meteorological measurement location; is it necessary to include this obstacle in the wind-tunnel model? Hunt (1974) showed that the velocity deficit in the wakes of cubes and cylinders is given approximately by:

$$DU_{mx}/U(h) = A\ (s/h)\text{-}3/2$$

downwind of the separation bubble, where DU_{mx} is the maximum mean velocity deficit created by the obstacle, h is the height of the obstacle, S is the distance downstream of the obstacle, and A is a constant dependent upon the obstacle shape, orientation, boundary layer thickness, etc. Typically, A = 2.5, but it may range from 1.5 to 5.0. If we desire that the velocity at the spill site be within 3 percent of its undisturbed value, Snyder (1981) recommends that any upstream obstacle as high as s/20 be included upstream in the model of the spill site. If the obstacle's width is much greater than its height (for example, a fence or ridge), one should include it in the physical model if its height is greater than s/100.

Blockage effects:

Because of the influence of wind-tunnel walls on the behavior of the flow past models, it is desirable to use small models or big tunnels, or both. On the other hand, larger models are not only easier to work with, but they may be needed for similarity reasons to achieve large enough Reynolds numbers. It is possible to identify three different types of effects of wind-tunnel constraints. The first is the simple "solid blockage" effect which arises because the fluid stream is unable to expand laterally as it normally would in unconfined flow. The second effect, called "wake blockage", results because the accelerated flow between an obstacle and the tunnel walls continues to "pinch" the wake flow region and reduce its normal lateral rate of growth. The third effect is produced by the growth of boundary layers on the tunnel walls which produce "wall boundary interference." Tunnel blockage can cause separation and reattachment locations to vary, produce higher velocities, larger wake turbulence, and modify the dispersion patterns in the vicinity of obstructions.

The ratio of the cross-sectional area of a model obstacle to that of the tunnel is called the "blockage ratio", BR. Mass continuity produces an average velocity speed-up of S = BR/(1-BR). Although wind tunnels with adjustable ceilings can compensate to some extent by raising the roof locally; this is not a perfect solution to the problem. Measurements on building and cooling tower models placed in different size wind-tunnel test sections reveal major changes in the character of pressure distributions, separation, and wake growth in the presence of flow restricted by wind-tunnel side walls (Farell et al., 1977).

Blockage corrections, which are conventionally applied in aeronautical tunnels, cannot usually be applied to the typical asymmetric model configuration placed against the wall of a meteorological wind tunnel (Ranga Raju and Singh, 1976). Conventional wisdom now suggests the "rule of thumb" that blockage ratios greater than five percent should be avoided.

Simulation of the flow over sharp-edged obstacles:

A number of authors have discussed flow studies about simple cubical or rectangular sharp-edged obstacles. An extensive review about such flow fields and the subsequent character of diffusion near obstacles has been provided by Hosker (1984). Peterka, Meroney and Kothari (1985) describe typical flow deviations which result from the presence of a sharp-edged building.

Consider the main features of the flow around a sharp-edged building. Typically, when the approach flow is normal to the building face, the flow separates from the ground upwind of the building and produces a "horseshoe"-shaped vortex which wraps around the base of the building. The surface streamline reattaches on the front of the building, and fluid parcels move up and down the building's forward face. An elevated streamline flows over the obstacle, dips down behind, and stagnates on the surface at the end of the recirculating cavity immediately downwind of the building. Sometimes separation streamlines from the forward building edges reattach to the same face, yet in other cases the streamlines enter the downwind cavity and mingle with the other recirculating fluid. Air which enters the cavity departs through turbulent mixing across the dividing streamlines, mingles with downwind-pointing vortices and is ejected laterally out of the cavity, or leaves suddenly during an exhalation when the entire cavity appears to collapse and then reform.

When a building is oriented obliquely to the wind, flow over the front side walls does not separate, but strong recirculation occurs on the downwind faces. Flow over the roof often produces counter-rotating "delta-wing" vortices which increase mixing over the top and in the wake of the building. These vortices can cause reattachment of the flow in the middle of the roof and serious plume downwash in the near wake. Other features of the flow near the building include vertical vortices produced by the vertical corners of the building.

Golden (1961) measured the concentration patterns above the roof of model cubes in a wind tunnel. Two sizes of cubes were used to vary the Reynolds number from 1000 to 94,000. The concentration isopleths in the fluid above the cube roof showed only slight variations over the entire range of Reynolds numbers studied. The maximum concentration on the roof itself was found to vary strongly with Reynolds numbers less than 11,000, but to be invariant with Reynolds numbers between 11,000 and 94,000. Frequently, modelers quote Golden's experiments as justification for presuming dispersion invariance when obstacle Reynolds numbers exceed 11,000. However, Golden's "11,000 rule" is limited to the measurement of

concentrations at only one point on the roof of smooth-walled cubes placed in a uniform approach flow of very low turbulent intensity. It is probably quite conservative because the shear and high turbulence in a simulated atmospheric boundary layer are likely to further reduce the critical Reynolds number. Indeed, Halitsky (1968) observed that for dispersion in the wake region, no change in isoconcentration isopleths from passive gas releases was found to occur for values of Reynolds number as low as 3300.

Flow around sharp-edged obstacles will remain kinematically similar at very low Reynolds numbers. Wake width variation will be minimal, and obstacle generated turbulence scales and intensity will only vary slowly as Reynolds number decreases. Gas clouds dispersing in this environment will remain similar at very low model speeds.

Simulation of flow over rounded obstacles:

Flow around a smooth cylinder is Reynolds number dependent. This dependence reflects changes in the nature of the boundary layer that forms over the cylinder and its behavior in the vicinity of the flow separation. At low Reynolds numbers, the boundary layer is laminar, and separation occurs easily under the influence of even modest positive pressure gradients. At higher Reynolds numbers, the boundary layer becomes turbulent and flow separation is delayed; i.e., the flow can move farther along a curved surface without separation. At prototype scales, obstacles are large enough that only turbulent separation occurs. However, model flows are usually at such low Reynolds numbers that the local boundary layer growing over a curved surface would be laminar. Most modelers attempt the reproduction of full- scale similarity around curved surfaces by artificially roughening the model surface to force transition to turbulence in these laminar boundary layers. This can be done by providing the surface with special (or artificial) roughness elements, for example, sandpaper, thin wires, or grooves. The height of the roughness, k, should be such that $Uk/\nu > 400$ and $k/R < 0.01$, where U is the mean wind speed at obstacle height, and R is the characteristic obstacle radius of curvature. Szechenyi (1975) studied flows about rough circular cylinders and determined that as Reynolds number decreases, roughening the surface becomes less effective. Fage and Warsap (1929) considered the effect of increasing the surface roughness of cylinders on their drag coefficient. Eventually, even ridiculously large roughness is ineffective.

Niemann and Ruhwedel (1980) compared pressures and forces about a 1:333 scale model to a full-scale hyperbolic cooling tower shell. They roughened their model with vertical ribs of height 0.09 mm and width 0.77 mm, producing a roughness coefficient of $k/2R = 0.0006$ and roughness Reynolds number, $Re_k > 270$. They found meridional forces on the cooling tower model and prototype were similar. Model Reynolds numbers were between $4.5*10^5$ and $6.0*10^5$, and this corresponding to $U_m > 45$ m/s. But again these speeds are much higher than is appropriate for current measurements.

Halitsky et al. (1963) examined dispersion about a smooth-model nuclear reactor containment building (a hemisphere fitted on a vertical cylinder) and found a critical Reynolds number greater than 79,000. (Yet this critical Reynolds number was for flow very close to the vessel wall. The behavior of concentration isopleths further downwind is likely to be less Reynolds number dependent.)

Although the details of fluid motions around rounded obstacles vary significantly with Reynolds number, the gross features of the flow do not change. Even small models at low wind speeds will produce horseshoe-shaped ground vortices, elevated pairs, and regular vortex shedding. If the internal boundary layer over the obstacle is laminar, then the wake region will be broader and less intense.

A.2.2 Performance of Prior Fluid Modeling Experiments

A number of studies have been performed in the Colorado State University Fluid Dynamics and Diffusion Laboratory to establish the effect of buildings and meteorological masts on flow fields. Hatcher et al. (1977) examined flow and dispersion in stratified flow downwind of the Experimental Organic Cooled Reactor, Idaho Falls; Allwine et al. (1978) studied the Rancho Seco Reactor, Sacramento; Kothari et al. (1981) studied the Duane Arnold Energy Center, Iowa. In each case field measurements were compared to laboratory measurements with good agreement. Specific effects of the structure of a meteorological mast on instrumentation response were reported by Hsi and Cermak (1965).

A.3 PHYSICAL MODEL OF PLUME MOTION

In addition to modeling the turbulent structure of the atmosphere in the vicinity of a test site it is necessary to properly scale the plume source conditions. One approach would be to follow the methodology used in Section 2.1; i.e., writing the conservation statements for the combined flow system followed by fractional analysis to find the governing parameters. An alternative approach, the one which will be used here, is that of similitude (Kline, 1965). The method of similitude obtains scaling parameters by reasoning that the mass ratios, force ratios, energy ratios, and property ratios should be equal for both model and prototype. When one considers the dynamics of gaseous plume behavior the following nondimensional parameters of importance are identified.[1]

$$\text{Mass Flux Ratio} = \frac{\text{mass flow of plume}}{\text{effective mass flow of air}}$$

[1] The scaling of plume Reynolds number is also a significant parameter. Its effects are invariant over a large range. This makes it possible to accurately model its influence by maintaining model tests above a minimum plume Reynolds number requirement.

Momentum Flux Ratio = $\frac{\text{inertia of plume}}{\text{effective inertia of air}}$

Densimetric Froude No. (relative to the inertia of the air) = $\frac{\text{effective inertia of air}}{\text{buoyancy of plume}}$

Densimetric Froude No. (relative to the inertia of the plume) = $\frac{\text{inertia of plume}}{\text{buoyancy of plume}}$

Flux Froude No. = $\frac{\text{momentum flux of air}}{\text{buoyancy momentum flux of plume}}$

Volume Flux Ratio = $\frac{\text{volume flow of plume}}{\text{effective volume flow of air}}$

It is necessary to maintain equality of the plume's specific gravity, ρ_g/ρ_a, over the plume's entire lifetime to obtain simultaneous simulation of all of these parameters. Unfortunately a requirement for equality of the plume gas specific gravity for plume with significant buoyancy differences (i.e. ρ_g not equal ρ_a) leads to several complications in practice. These are:

1) Equality of the source gas specific gravity between a model and its atmospheric equivalent leads to a wind speed scaling from $(U_m/U_p)^2 = L_m/L_p$. For a significant range of atmospheric wind speeds this relationship leads to wind- tunnel speeds at which there is a possible loss of the Reynolds number invariance in the approach flow.

2) A thermal plume in the atmosphere is frequently simulated in the laboratory by an isothermal plume formed from a gas of appropriate molecular weight. Under certain situations of specific heat capacity mismatch, this practice will lead to a variation of the equality of plume density as the plume mixes with air.

It is important to examine each modeling situation and decide if an approximation to complete plume behavior may be employed without a significant loss in the similarity of the modeled plume structure.